DIMENSION REDUCTION OF HYPERSPECTRAL IMAGES

PROJECT REPORT

Submitted by

DEEPA P

Register No: 13MCO05

in partial fulfillment for the requirement of award of the degree

of

MASTER OF ENGINEERING

in

COMMUNICATION SYSTEMS

Department of Electronics and Communication Engineering

KUMARAGURU COLLEGE OF TECHNOLOGY

(An autonomous institution affiliated to Anna University, Chennai)

COIMBATORE - 641 049

ANNA UNIVERSITY: CHENNAI 600 025

APRIL 2015

BONAFIDE CERTIFICATE

Certified that this project report titled **"DIMENSION REDUCTION OF HYPERSPECTRAL IMAGES"** is the bonafide work of **DEEPA.P [Reg. No. 13MCO05]** who carried out the research under my supervision. Certified further, that to the best of my knowledge the work reported herein does not form part of any other project or dissertation on the basis of which a degree or award was conferred on an earlier occasion on this or any other candidate.

SIGNATURE

Ms.K.THILAGAVATHI

PROJECT SUPERVISOR

Department of ECE

Kumaraguru College of Technology

Coimbatore-641 049

SIGNATURE

Dr. RAJESWARI MARIAPPAN

HEAD OF THE DEPARTMENT

Department of ECE

Kumaraguru College of Technology

Coimbatore-641 049

The Candidate with university **Register No. 13MCO05** was examined by us in the project viva –voice examination held on .....

INTERNAL EXAMINER **EXTERNAL EXAMINER**

ACKNOWLEDGEMENT

First, I would like to express my praise and gratitude to the Lord, who has showered his grace and blessings enabling me to complete this project in an excellent manner.

I express my sincere thanks to the management of Kumaraguru College of Technology and Joint Correspondent **Shri. Shankar Vanavarayar** for the kind support and for providing necessary facilities to carry out the work.

I would like to express my sincere thanks to our beloved Principal **Dr.R.S.Kumar Ph.D.,** Kumaraguru College of Technology, who encouraged me with his valuable thoughts.

I would like to thank **Dr.Rajeswari Mariappan Ph.D.,** Head of the Department, Electronics and Communication Engineering, for her kind support and for providing necessary facilities to carry out the project work.

In particular, I wish to thank with everlasting gratitude to the project coordinator **Ms.R.Hemalatha M.E., (Ph.D)** Associate Professor, Department of Electronics and Communication Engineering ,for her expert counselling and guidance to make this project to a great deal of success.

I am greatly privileged to express my heartfelt thanks to my project guide **Ms.K.Thilagavathi M.E.,** Asst. Professor (SRG), Department of Electronics and Communication Engineering, throughout the course of this project work and I wish to convey my deep sense of gratitude to all teaching and non-teaching staff of ECE Department for their help and cooperation.

Finally, I thank my parents and my family members for giving me the moral support and abundant blessings in all of my activities and my dear friends who helped me to endure my difficult times with their unfailing support and warm wishes.

ABSTRACT

Hyperspectral data sets are generally composed of about 100 to 200 spectral bands of relatively narrow bandwidths (5-10 nm). Hyperspectral data can be represented using a cube and new challenges arise in dealing with extremely large datasets. Feature extraction and dimension reduction in hyperspectral imaging can be done by various techniques. Popular dimensionality-reduction technique such as principal component analysis (PCA) has high computational cost and large memory requirement when used with hyperspectral images. The proposed method is Folded-PCA, where the spectral vector is folded into a matrix to allow the covariance matrix to be determined more efficiently. An algorithm has been developed to find the intrinsic dimensionality of hyperspectral image. Also, denoising of dimension reduced image is done for its better visualization. Folded-PCA takes into account both global and local structures thus providing additional information. Moreover, both the computational cost and the memory requirement have been significantly reduced. A comparative analysis of PCA, Segmented-PCA and F-PCA has been carried out.

TABLE OF CONTENTS

LIST OF FIGURES

LIST OF TABLES

LIST OF ABBREVIATIONS

ASF	Alternated Sequential Filters
AVIRIS	Airborne Visible Infrared Imaging Spectrometer
DCT	Discrete Cosine Transform
DWT	Discrete Wavelet Transform
EDMP	Extended Differential Morphological Profile
FFT	Fast Fourier Transform
F-PCA	Folded Principal Component Analysis
GMM	Gaussian Mixture Model
HSI	Hyperspectral Imaging
HYDICE	Hyperspectral Digital Imagery Collection Experiment
ICA	Independent Component Analysis
IG	Information Gain
ISOMAP	Isometric mapping
LDA	Linear Discriminant Analysis
LFDA	Local Fisher's Discriminant Analysis
LLE	Locally Linear Embedding
LPP	Locality-Preserving Projections
MCRD	Minimum Change Rate Deviation
MNF	Maximum Noise Fraction
NIR	Near Infrared Microscopy
PCA	Principal Component Analysis
PSNR	Peak Signal to Noise Ratio
ROD	Rose of Directions
SAR	Synthetic Aperture Radar
SMMS	Small Multi-Mission Satellite

SOMP	Scale Orientation Morphological Profiles
SSIM	Structural Similarity Index
SVD	Singular Value Decomposition
SVM	Support Vector Machine
SWIR	Short Wavelength Infrared
VNIR	Visible and Near Infrared

€

CHPTER 1

INTRODUCTION

1.1 OVERVIEW

Remote sensing is the science of acquiring information about the Earth's surface without actually being in contact with it. This is done by sensing and recording reflected or emitted energy and processing, analyzing, and applying that information. Remote sensing is based on the measurement of reflected or emitted radiation from different bodies. Objects having different surface features reflect or absorb the sun's radiation in different ways. The reflectance properties of an object depend on the particular material and its physical and chemical state (e.g. moisture), the surface roughness as well as the geometric circumstances (e.g. incidence angle of the sunlight). The most important surface features are colour, structure and surface texture. These differences make it possible to identify different earth surface features or materials by analyzing their spectral reflectance patterns or spectral signatures. These signatures can be visualized in so called spectral reflectance curves as a function of wavelength.

The primary prerequisite for remote sensing is to have a vitality source to light up the target (unless the sensed vitality is being radiated by the target). This vitality is as electromagnetic radiation. All electromagnetic radiation has key properties and carries on in unsurprising routes as indicated by the fundamentals of wave hypothesis. Electromagnetic radiation comprises of an electrical field (E) which fluctuates in size in a bearing opposite to the course in which the radiation is voyaging, and an attractive field (M) situated at right plot to the electrical field. Both these fields go at the pace of light (c). Fig. 1.1 shows EM wave.

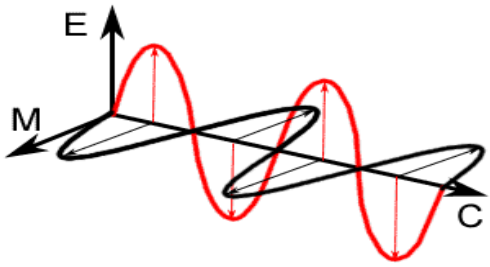

Figure.1.1 Electromagnetic wave

The electromagnetic spectrum ranges from the shorter wavelengths (counting gamma and x-beams) to the more extended wavelengths (counting microwaves and telecast radio waves). There are a few locales of the electromagnetic range which are helpful for remote sensing. For most purposes, the bright or UV part of the range has the briefest wavelengths. This radiation is simply past the violet share of the noticeable wavelengths, thus its name. Some Earth surface materials, essentially shakes and minerals, fluoresce or radiate unmistakable light when lit up by UV radiation. Electromagnetic waves utilized as a part of remote sensing is demonstrated in Fig.1.2.

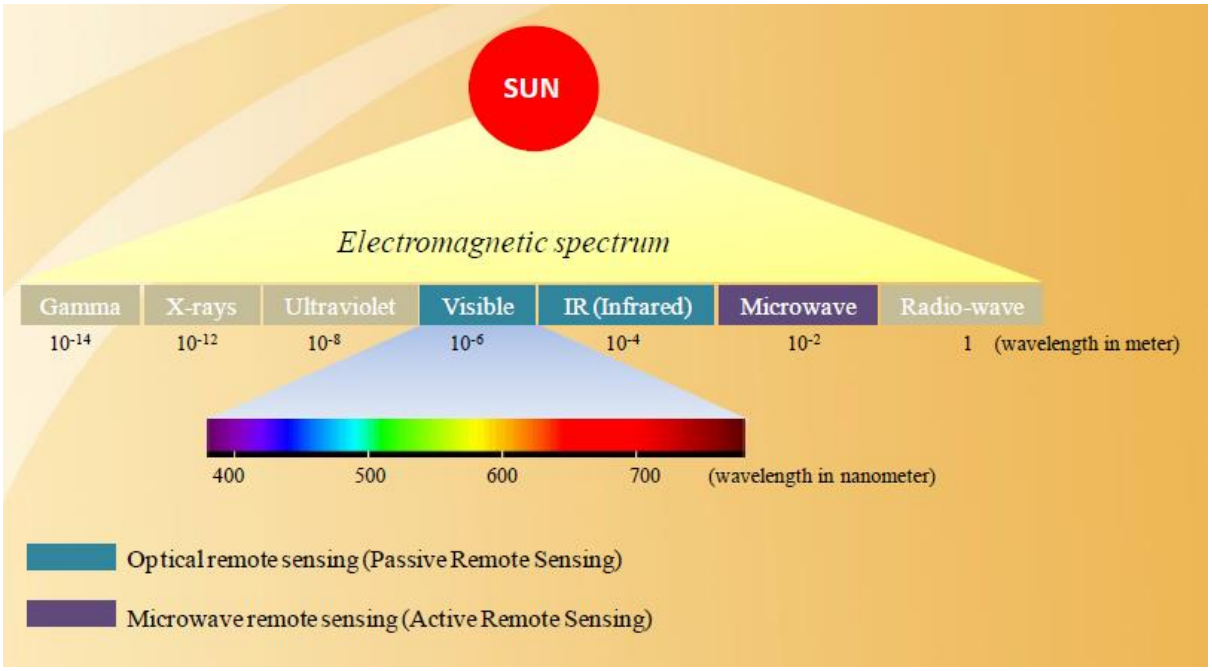

Figure.1.2 Electromagnetic spectrum

There are two main types of remote sensing: Passive remote sensing and Active remote sensing. Passive sensors detect natural radiation that is emitted or reflected by the object or surrounding area being observed. Reflected sunlight is the most common source of radiation measured by passive sensors. Examples of passive remote sensors include film photography, infrared, and radiometers. Passive remote sensing is illustrated in Fig.1.3.

Active remote sensing, on the other hand, emits energy in order to scan objects and areas whereupon a sensor then detects and measures the radiation that is reflected or backscattered from the target. RADAR is an example of active remote sensing where the time delay between emission and return is measured, establishing the location, height, speeds and direction of an object. Active remote sensing is illustrated in Fig.1.4.

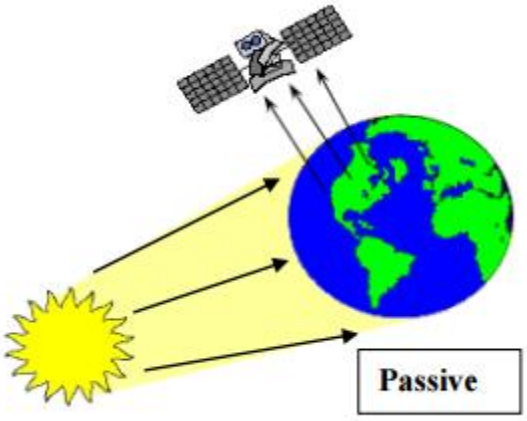

Figure.1.3 Passive remote sensing

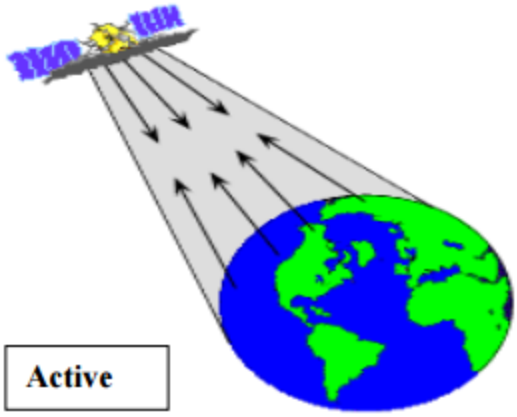

Figure.1.4 Active remote sensing

Remote sensing finds application in areas such as agriculture, forestry, urbanization and transportation, natural resource management, geology, hydrology, land cover, mapping etc. Each sensor is designed with a specific purpose. With optical sensors, the design focuses on the spectral bands to be collected. With radar imaging, the incidence angle and microwave band used plays an important role in defining which applications the sensor is best suited for. Each application itself has specific demands, for spectral resolution, spatial resolution, and temporal resolution.

Our eyes only see visible band of the light spectrum. Many more bands of non-visible light exist to the left and right of visible spectrum. **Hyperspectral Imaging (HSI)** is a technology

which divides regions of those spectra which we can't see into many more bands and creates visible images from them.

1.2 HYPERSPECTRAL IMAGING

A hyperspectral image (HSI), in general, has hundreds of spectral bands in contrast to a normal digital image which has three spectral bands (blue, red, and green) and thus offers a more complete part of the light spectrum for viewing and analysis. In general, hyperspectral sensors measure bands at 10 to 20 nm intervals. This high dimensionality makes HSI good candidates for the methods of dimensionality reduction. A regular digital image can be viewed as a collection of three-dimensional spectral vectors, each representing the information for one pixel. Similarly a hyper-spectral image can be viewed as a collection of D-dimensional spectral vectors, each representing the information for one pixel. Hyperspectral images typically include spectral bands representing the ultraviolet (200-400 nm), visible (400-700 nm), near infrared (700-1000 nm), and short-wave infrared (1000- 4000 nm). Thus, HSI are favoured over regular images for some applications such as forestry and crop analysis, mineral exploration, and surveillance. Hyperspectral image cube structure is illustrated in Fig.1.5. Each pixel has intensity values corresponding to all spectral bands, as shown in Fig.1.6

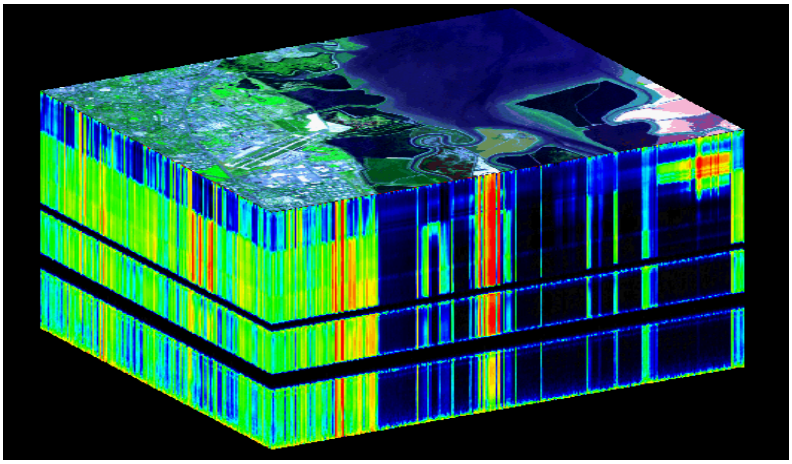

Figure.1.5 Hyperspectral image cube

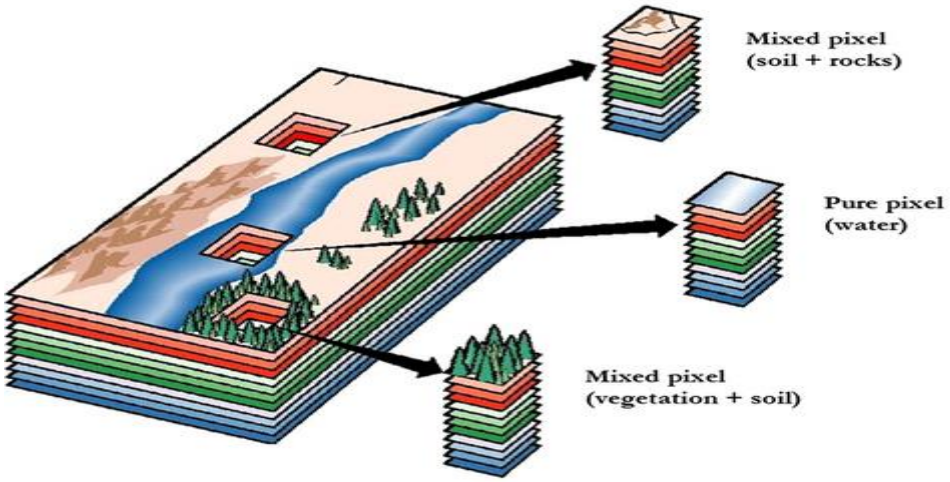

Figure.1.6 Hyperspectral image structure

1.2.1 Distinguishing Hyperspectral from Multispectral Imaging

Hyperspectral imaging is part of a class of techniques commonly referred to as spectral imaging or spectral analysis. Hyperspectral imaging is related to multispectral imaging. The distinction between hyper- and multi-spectral is sometimes based on an arbitrary "number of bands" or on the type of measurement, depending on what is appropriate to the purpose.

Multispectral imaging deals with several images at discrete and somewhat narrow bands. Being "discrete and somewhat narrow" is what distinguishes multispectral in the visible from colour photography. A multispectral sensor may have many bands covering the spectrum from the visible to the long wave infrared. Multispectral images do not produce the "spectrum" of an object. Landsat is an excellent example of multispectral imaging.

Hyperspectral deals with imaging narrow spectral bands over a continuous spectral range, and produce the spectra of all pixels in the scene. So a sensor with only 20 bands can also be hyperspectral when it covers the range from 500 to 700 nm with 20 bands each 10 nm wide. (While a sensor with 20 discrete bands covering the VIS, NIR, SWIR, MWIR, and LWIR would be considered multispectral.)

'Ultraspectral' could be reserved for interferometer type imaging sensors with a very fine spectral resolution. These sensors often have a low spatial resolution of several pixels only, a restriction imposed by the high data rate.

1.2.2 Applications

Hyperspectral remote sensing is used in a wide array of applications. Although originally developed for mining and geology (the ability of hyperspectral imaging to identify various minerals makes it ideal for the mining and oil industries, where it can be used to look for ore and oil), it has now spread into fields as widespread as ecology and surveillance, as well as historical manuscript research, such as the imaging of the Archimedes Palimpsest. This technology is continually becoming more available to the public. Organizations such as NASA and the USGS have catalogues of various minerals and their spectral signatures, and have posted them online to make them readily available for researchers.

- **Agriculture**

Although the cost of acquiring hyperspectral images is typically high, for specific crops and in specific climates, hyperspectral remote sensing use is increasing for monitoring the development and health of crops. In Australia, work is under way to use imaging spectrometers to detect grape variety and develop an early warning system for disease outbreaks. Furthermore, work is underway to use hyperspectral data to detect the chemical composition of plants, which can be used to detect the nutrient and water status of wheat in irrigated systems.

Another application in agriculture is the detection of animal proteins in compound feeds to avoid bovine spongiform encephalopathy, also known as mad-cow disease. Different studies have been done to propose alternative tools to the reference method of detection, (classical microscopy). One of the first alternatives is near infrared microscopy (NIR), which combines the advantages of microscopy and NIR. In 2004, the first study relating this problem with hyperspectral imaging was published. Hyperspectral libraries that are representative of the diversity of ingredients usually present in the preparation of compound feeds were constructed. These libraries can be used together with chemometric tools to investigate the limit of detection, specificity and reproducibility of the NIR hyperspectral imaging method for the detection and quantification of animal ingredients in feed.

- **Eye care**

Researchers at the Université de Montréal are working with Photon etc. and Optina Diagnostics to test the use of hyperspectral photography in the diagnosis of retinopathy and

macular edema before damage to the eye occurs. The metabolic hyperspectral camera will detect a drop in oxygen consumption in the retina, which indicates potential disease. An ophthalmologist will then be able to treat the retina with injections to prevent any potential damage.

- **Food processing**

In the nourishment transforming industry, hyperspectral imaging, consolidated with wise programming, empowers computerized sorters (additionally called optical sorters) to distinguish and uproot imperfections and remote material (FM) that are imperceptible to conventional cam and laser sorters. By enhancing the exactness of deformity and FM evacuation, the nourishment processor's goal is to improve item quality and expand yields.

Receiving hyperspectral imaging on computerized sorters accomplishes non-ruinous, 100 percent review in-line at full generation volumes. The sorter's product contrasts the hyperspectral pictures gathered with client characterized acknowledge/reject edges, and the discharge framework naturally uproots imperfections and outside material.

The late business appropriation of hyperspectral sensor-based nourishment sorters is most exceptional in the nut business where introduced frameworks augment the evacuation of stones, shells and other remote material (FM) and unessential vegetable matter (EVM) from walnuts, pecans, almonds, pistachios, peanuts and different nuts. Here, enhanced item quality, low false reject rates and the capacity to handle high approaching deformity stacks frequently support the expense of the innovation.

Business appropriation of hyperspectral sorters is likewise propelling at a quick pace in the potato handling industry where the innovation guarantees to tackle various exceptional item quality issues. Work is in progress to utilize hyperspectral imaging to identify "sugar closures," "empty heart" and "normal scab," conditions that torment potato processors.

- **Mineralogy**

Geographical specimens, for example, drill centers, can be quickly mapped for almost all minerals of business enthusiasm with hyperspectral imaging. Combination of SWIR and LWIR unearthly imaging is standard for the recognition of minerals in the feldspar, silica, calcite, garnet, and olivine bunches, as these minerals have their most unique and strongest ghastly signature in the LWIR districts.

Hyperspectral remote sensing of minerals is decently created. Numerous minerals can be recognized from airborne pictures, and their connection to the vicinity of profitable minerals, for example, gold and precious stones, is well caught on. At present, advancement is towards understanding the relationship in the middle of oil and gas spillages from pipelines and regular wells, and their consequences for the vegetation and the ghastly marks.

- **Surveillance**

Hyperspectral warm infrared emanation estimation, an open air examine in winter conditions, encompassing temperature -15°C—relative brilliance spectra from different focuses in the picture are indicated with bolts. The infrared spectra of the distinctive protests, for example, the watch glass have obviously unique qualities. The difference level demonstrates the temperature of the article. This picture was created with a Specim LWIR hyperspectral imager.

Hyperspectral reconnaissance is the usage of hyperspectral filtering innovation for observation purposes. Hyperspectral imaging is especially helpful in military reconnaissance as a result of countermeasures that military elements now take to dodge airborne observation. Aeronautical reconnaissance was utilized by French officers utilizing fastened blow ups to keep an eye on troop developments amid the French Revolutionary Wars, and since that time, warriors have taken in to escape the exposed eye, as well as to cover their warmth marks to mix into the surroundings and maintain a strategic distance from infrared examining. The thought that drives hyperspectral reconnaissance is that hyperspectral examining draws data from such a vast allotment of the light range that any given article ought to have an extraordinary ghastly signature in no less than a couple of the numerous groups that are filtered.

Customarily, monetarily accessible warm infrared hyperspectral imaging frameworks have required fluid nitrogen or helium cooling, which has made them unreasonable for most observation.

- **Physics**

Physicists use an electron microscopy technique that involves microanalysis using energy-dispersive X-ray spectroscopy (EDS), electron energy loss spectroscopy (EELS), infrared spectroscopy (IR), Raman spectroscopy, or cathodoluminescence (CL) spectroscopy, in which the entire spectrum measured at each point, is recorded. EELS hyperspectral imaging is performed in a

scanning transmission electron microscope (STEM); EDS and CL mapping can be performed in STEM as well, or in a scanning electron microscope or electron microprobe (also called an electron probe microanalyzer or EPMA). Often, multiple techniques (EDS, EELS, CL) are used simultaneously.

In a "normal" mapping experiment, an image of the sample is simply the intensity of a particular emission mapped in an XY raster. For example, an EDS map could be made of a steel sample, in which iron X-ray intensity is used for the intensity gray scale of the image. Dark areas in the image would indicate non-iron-bearing impurities. This could potentially give misleading results; if the steel contained tungsten inclusions, for example, the high atomic number of tungsten could result in bremsstrahlung radiation that would make the iron-free areas appear to be rich in iron.

By hyperspectral mapping, instead, the entire spectrum at each mapping point is acquired, and a quantitative analysis can be performed by computer post processing of the data, and a quantitative map of iron content produced. This would show which areas contained no iron, despite the anomalous X-ray counts caused by bremsstrahlung. Because EELS core-loss edges are small signals on top of a large background, hyperspectral imaging allows large improvements to the quality of EELS chemical maps.

Similarly, in CL mapping, small shifts in the peak emission energy could be mapped, which would give information regarding slight chemical composition changes or changes in the stress state of a sample.

- **Astronomy**

In astronomy, hyperspectral imaging is used to determine a spatially-resolved spectral image. Since a spectrum is an important diagnostic, having a spectrum for each pixel allows more science cases to be addressed. In astronomy, this technique is commonly referred to as integral field spectroscopy, and examples of this technique include FLAMES and SINFONI on the Very Large Telescope, but also the Advanced CCD Imaging Spectrometer on Chandra X-ray Observatory uses this technique.

- **Chemical imaging**

Soldiers can be exposed to a wide variety of chemical hazards. These threats are mostly invisible but detectable by hyperspectral imaging technology. The Telops Hyper-Cam, introduced in 2005, has demonstrated this at distances up to 5 km and with concentrations as low as a few ppm.

- **Environment**

Most countries require continuous monitoring of emissions produced by coal and oil-fired power plants, municipal and hazardous waste incinerators, cement plants, as well as many other types of industrial sources. This monitoring is usually performed using extractive sampling systems coupled with infrared spectroscopy techniques. Some recent standoff measurements performed allowed the evaluation of the air quality but not many remote independent methods allow for low uncertainty measurements.

1.2.3 Special Issues in Hyperspectral Imagery

Although the potential of hyperspectral remote sensing is exciting, there are special issues that arise with this unique type of imagery. For example, many hyperspectral analysis algorithms require accurate atmospheric corrections to be performed. To meet this need, sophisticated atmospheric correction algorithms have been developed to calculate concentrations of atmospheric gases directly from the detailed spectral information contained in the imagery itself without additional ancillary data. These corrections can be performed separately for each pixel because each pixel has a detailed spectrum associated with it. Several of these atmospheric correction algorithms are available within commercial image processing software. However, several image analysis algorithms have been successfully used with uncorrected imagery. For example, the BandMax tool owned by the Galileo Group has been widely used with radiance imagery.

Many hyperspectral analysis approaches require the use of known material spectra. Known spectra can guide spectral classifications or define targets to use in spectral image analysis. Some investigators collect spectral libraries for materials in their field sites as part of every project. Several high quality spectral libraries are also publicly available. Some investigators derive spectral libraries from the image to be analyzed using specially designed algorithms available in

commercial software. This approach ensures that the spectra will always be exactly comparable to the image pixel spectra.

Finally, hyperspectral imagery is often not as readily available as other types of remotely sensed data. In particular, there are few spaceborne hyperspectral sensors. Nevertheless, several recently launched hyperspectral sensors are acquiring imagery from space, including the Hyperion sensor on NASA's EO-1 satellite, the CHRIS sensor on the European Space Agency's PROBA satellite, and the FTHSI sensor on the U.S. Air Force Research Lab's MightySat II satellite. The EROS Data Center is currently providing Hyperion imagery at a relatively low cost to the general public (http://edc.usgs.gov/ products/satellite/eo1.html). Many airborne hyperspectral sensors, including NASA's AVIRIS sensor, are also available to collect data.

1.2.4 Hyperspectral Image Sensors

The timeline in Fig.1.7 illustrates that high-spatial-resolution (≤ 30 m) hyperspectral sensing has been implemented on a number of experimental airborne platforms, including the Hyperspectral Digital Imagery Collection Experiment (HYDICE) and the Airborne Visible Infrared Imaging Spectrometer (AVIRIS). EO-1 carries a hyperspectral sensor called Hyperion. Comparison of the three sensors in terms of various parameters is given in table 1.1.

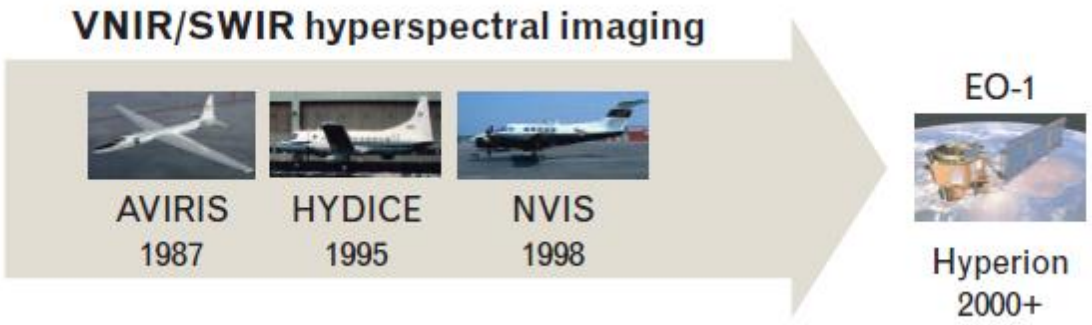

Figure.1.7 Timeline highlighting hyperspectral imaging sensors

Table.1.1. Comparison of hyperspectral imaging systems

Parameter	HYDICE	AVIRIS	Hyperion
Nominal altitude (km)	1.6	20	705
Swath (km)	0.25	11	7.6
Spatial resolution (m)	0.75	20	30
Spectral coverage (μm)	0.4-2.5	0.4-2.5	0.4-2.5
Spectral resolution (nm)	7-14	10	10
Number of bands	210	224	242
Focal-plane pixels (spatial x spectral)	320 x 210	614 x 224	256 x 242
Data-cube size	300x320x210	512x614x224	660x256x242
Cube collection time (sec)	3	43	3

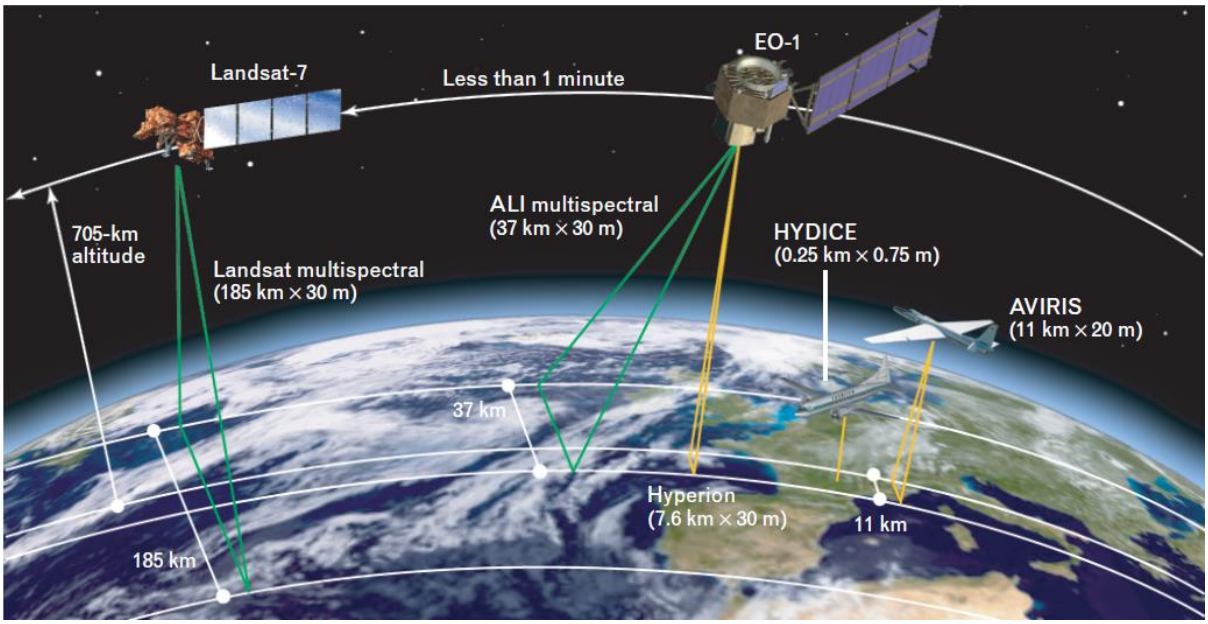

Figure.1.8 Altitude and area coverage regions for HYDICE, AVIRIS, and Hyperion (on EO-1) hyperspectral sensor platforms

Altitude and area coverage regions for HYDICE, AVIRIS, and Hyperion (on EO-1) hyperspectral sensor platforms are illustrated in Fig.1.8. The nominal swath width and spatial resolution of each sensor are shown in parentheses. The difference in swath width between the mature operational Landsat-7 multispectral sensor (185 km) and the experimental hyperspectral

sensors—HYDICE (0.25 km), AVIRIS (11 km), and Hyperion (7.6 km) are obvious from the figure. Hyperspectral images captured by Hyperion and AVIRIS has been used for the experiment. The detailed description of these two sensors is given below.

- **Hyperion**

The Hyperion gives a science evaluation instrument with quality adjustment in view of legacy from the LEWIS Hyperspectral Imaging Instrument (HSI). The Hyperion capacities give determination of surface properties into several unearthly groups versus the ten multispectral groups flown on customary Landsat imaging missions. Through these ghostly groups, complex area eco-frameworks can be imaged and precisely grouped. The Hyperion gives a high determination hyperspectral imager equipped for determining 220 unearthly groups (from 0.4 to 2.5 μm) with a 30-meter determination. The instrument can picture a 7.5 km by 100 km land region every picture, and give point by point ghastly mapping over each of the 220 channels with high radiometric precision. The significant parts of the instrument include the following:

- Framework fore-optics configuration in light of the Korea Multi-Purpose Satellite (KOMPSAT) Electro Optical Camera (EOC) mission. The telescope accommodates two different grinding picture spectrometers to enhance signal to noise ratio (SNR).

The benefits of Hyperion sensor include a focal plane array which provides separate Short Wavelength Infrared (SWIR) and Visible and Near Infrared (VNIR) detectors based on spare hardware from the LEWIS HSI program and a cryocooler indistinguishable to that created for the LEWIS HSI mission for cooling of the SWIR central plane. Hyperspectral imaging has boundless applications in mining, topography, ranger service, agribusiness, and natural administration.

- **AVIRIS**

AVIRIS is a proven instrument in the realm of Earth Remote Sensing. It is a unique optical sensor that delivers calibrated images of the upwelling spectral radiance in 224 contiguous spectral channels (bands) with wavelengths from 400 to 2500 nanometers. AVIRIS has been flown on four aircraft platforms: NASA's ER-2 jet, Twin Otter International's turboprop, Scaled Composites' Proteus, and NASA's WB-57. The ER-2 flies at approximately 20 km above sea level, at about 730 km/hr. The Twin Otter aircraft flies at 4km above ground level at 130km/hr. AVIRIS has flown North America, Europe, portions of South America, and Argentina.

The main objective of the AVIRIS project is to identify, measure, and monitor constituents of the Earth's surface and atmosphere based on molecular absorption and particle scattering signatures. Research with AVIRIS data is predominantly focused on understanding processes related to the global environment and climate change.

1.2.5 Motivation and Problem Statement

In recent studies, Folded-PCA (F-PCA) as a dimensionality reducer has been used for hyperspectral image. But the effect of noise is to be eliminated. Motivated by this an algorithm is introduced that reduces the dimension. The intrinsic dimensionality has been determined based on the contribution of each component to the cumulative variance. Also de-noising concept has been introduced to eliminate the effect of noise.

1.2.6 Objectives

The main objective of the project is to reduce the dimension of hyperspectral images using Noise-adjusted Folded-PCA method with stopping rule. The sub objective is to compare the performance of the proposed algorithm with existing algorithms such as PCA and Segmented-PCA (Seg-PCA).

1.2.7 Need for Dimension Reduction

Dimensionality reduction is a field of mathematics that deals with the complexities of very large data sets and attempts to reduce the dimensionality of the data while preserving the important characteristics of the data. These algorithms are becoming more important today because the complexity of sensors have increased the ability to store massive amounts of data. For example, hyperspectral sensors record roughly a hundred times the amount of information as a typical optical sensor. The quantity of the bands of the hyperspectral image data is very large, and the correlation of the bands is quite strong, too. On one hand, the hugeness of the data brings difficulties to not only data storage, but also data processing. It holds back the applying of the hyperspectral image data in some degrees. On the other hands, traditional methods which have been designed for multi-spectral image data cannot be easily applied to hyperspectral image data. So, dimensional reduction in hyperspectral image data without losing important information about objects of interest is important. Basic idea of dimensionality reduction in hyperspectral image is shown in Fig.1.9.

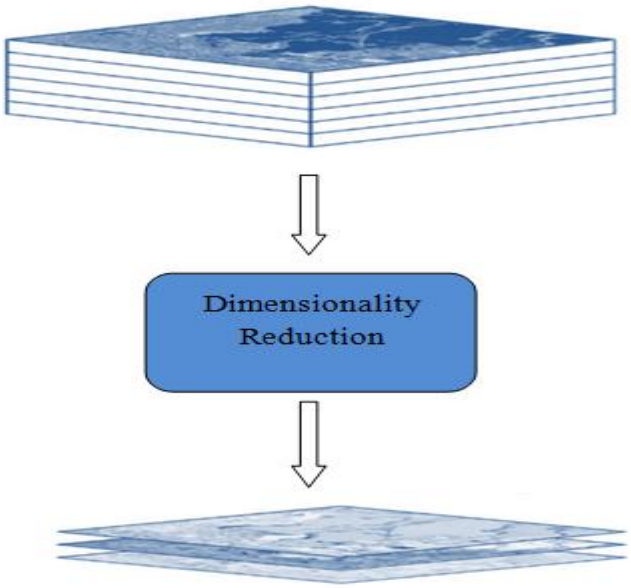

Figure.1.9 Dimension reduction of hyperspectral image

CHAPTER 2

LITERATURE SURVEY

Dimensionality Reduction of Hyperspectral Data Using Discrete Wavelet Transform Feature Extraction

Lori Mann Bruce, Cliff H. Koger, and Jiang Li

In this paper, the wavelet transform is presented for hyperspectral feature extraction and classification. Synthetic aperture radar (SAR), multispectral, and panchromatic data use wavelet transform for image compression, edge detection, and image fusion. Its inherent multiresolution nature makes the wavelet transform an important tool for feature extraction. Wavelet functions when applied to hyperspectral signal separate the fine-scale and large-scale information. This is done in an iterative fashion using the discrete wavelet transform (DWT). A varying width operator which is not restricted to being derivative is used for wavelet transform. The operator is referred to as the mother wavelet. Once a mother wavelet is selected, the wavelet transform can be used to separate the fine-scale information from the large-scale information.

In this paper, the DWT based feature extraction method is compared with conventional feature extraction methods. It is found that the classification accuracy is high compared to dimensionality reduction methods such as best spectral band selection and PCA. Also, the DWT method outperformed techniques, such as FFT- and DCT-based feature extraction that consider only frequency content of the signal and not localized information. The data obtained after applying wavelet based reduction technique has spectral distribution similar to the original distribution, but in a compressed form. Thus this method yields better classification accuracy than PCA.

The DWT based method is a lossy compression as only the approximation after Wavelet transform is kept for analysis and the removed high frequency signal may contain useful information for class separation and identification. When this method is used for land-cover classification, feature extraction is carried out without incorporating information on the spatially adjacent data.

Dimensionality Reduction and Classification of Hyperspectral Image Data Using Sequences of Extended Morphological Transformations

Antonio Plaza, Pablo Martínez, Javier Plaza, and Rosa Pérez

This paper focus on design of multichannel filters for analyzing spatial and spectral patterns simultaneously. Three morphological filtering techniques are explained in this paper: extended differential morphological profiles extended alternated sequential filters, and scale-orientation morphological profiles. In the first method an extended differential morphological profile (EDMP) is defined as a vector where a measure of the spectral variation of the multichannel opening-closing profile is stored for every step of an increasing series. Maximum derivative score in the opening series is obtained for pixels that are spectrally pure, whereas the maximum derivative score in the closing series is obtained for mixed pixels. Thus the information about the spectral purity of the pixel and the spatial distribution of the object in the scene are obtained.

Alternated sequential filters (ASFs) depend on reconstruction-based morphological operations. Image features are preserved in this method. EDMP approach ensures self-duality property. In ASF method the property may be lost based on whether the sequence is started with an opening or a closing by reconstruction filter.

Scale-orientation morphological profiles represent (SOMP) a line segment with minimal length and the analysis is based on the slope of the line. Rose of directions (ROD) is used to analyze the SOMP at a given pixel by plotting the opened and closed values versus the orientation of the line segment by using a polar diagram.

A drawback in the proposed approach is a heavy computational burden when processing high-dimensional data. This is caused by the need to have morphological filters with increasing scale and orientation feature.

Spatially Coherent Nonlinear Dimensionality Reduction and Segmentation of Hyperspectral Images.

Anish Mohan, Guillermo Sapiro, and Edward Bosch

The spatially coherent nonlinear dimensionality reduction technique called locally linear embedding (LLE) is investigated in this paper. The proposed method is critical for accurate classification and segmentation of hyperspectral image. Hyperspectral image consists of numerous continuous spectral bands. Each pixel is represented in the form of a vector called spectral vector. The high correlation among these spectral vectors is considered in LLE.

The first step in the algorithm is to calculate the neighbours of a pixel in a spatially coherent way. Then the pixel is represented as a linear combination of its local neighbours. The linear approximation in the neighbourhood is based on the calculation of weights that linearly reconstruct the data point from its spatial neighbours. LLE is called spatially coherent because the same spatial local neighbourhoods exist in the original high and lower projected dimensions. LLE follow Euclidean distance calculation. An alternative approach to calculate the distance between pixel vectors is also introduced in this paper. This is based on a distance matrix whose entries are proportional to the spatial (Euclidean) distance between pixels. This method has a problem if objects of the same class are spatially separated. The limitation of LLE is its poor efficiency when used with natural images.

Independent Component Analysis-Based Dimensionality Reduction with Applications in Hyperspectral Image Analysis

Jing Wang, and Chein-I Chang

An independent component analysis (ICA) approach to dimensionality reduction (DR), to be called ICA-DR is studied in this paper. The number of dimensions needed to be retained is estimated based on virtual dimensionality. The principal components analysis (PCA) and the maximum noise fraction (MNF) are most commonly used techniques for dimensionality reduction in hyperspectral images, referred to as PCA-DR and MNF-DR, respectively. There are two major

issues for these methods are the measurement of data that exceeds second-order statistics and the determination of number of dimensions to be retained. These issues are addressed by ICA-DR.

Independent components are generated using random initial projection vectors so there is no prioritization among components generated by the ICA-DR. Three algorithms are developed in this paper to introduce component prioritization. First algorithm called ICA-DR1 is based on virtual dimensionality. Another is called ICA-DR2 which implements the ICA as a random algorithm with randomness characterized by random initial projection vectors. The third algorithm called ICA-DR3 generate an appropriate set of initial projection vectors to replace random projection vectors used by the ICA with the use of a custom-designed initialization algorithm in conjunction with the virtual dimensionality.

The biggest disadvantage of ICA is that scale of resulting signal is not same as original data as it cannot estimate energy of result.

Exploiting Manifold Geometry in Hyperspectral Imagery

Charles M. Bachmann, Thomas L. Ainsworth, and Robert A. Fusina

Linear mixing and best band selection are the general methods for spectral analysis. These approaches do not consider the inherent nonlinear characteristics of hyperspectral data. An algorithm called Isometric mapping (ISOMAP) exploits the nonlinear structure of hyperspectral image. ISOMAP provides globally optimal solution. But computational burden is dominant in this algorithm. This paper introduces a hybrid technique to avoid ISOMAP's computational cost by applying scaling to large-scale remote sensing datasets. The approach here is to divide a large dataset to small tiles and manifold is derived from each tile. These results are aligned and stitched together to reconstruct the original scene. The second approach described involves random sampling of original data cube in order to generate small data cubes.

The limitations of ISOMAP are graph discreteness overestimates the geodesic distance (Shortest curve along the manifold connecting two points) and the dimension must be high to avoid "linear shortcuts" near regions of high surface curvature.

Dimension Reduction of Optical Remote Sensing Images via Minimum Change Rate Deviation Method

Rouhollah Dianat and Shohreh Kasaei

This paper describes dimension reduction techniques called minimum change rate deviation (MCRD). It considers the spatial relation among neighbouring pixels. The resulted components after PCA are uncorrelated with each other and the error decreases with the increasing number of components. These properties are preserved in minimum change rate deviation and it is shown that MCRD outperforms PCA in retaining the required information for classification purposes. Thus the main objective of this paper is to develop a linear – spatial oriented dimension reduction method. The main steps of the proposed MCRD methods are:

• First, apply a linear spatial-oriented image operator to the image

• Rearrange the selected features by assigning some priority.

• Calculate the *i*th reduced image so that its related features for each point are as close as possible to the *i*th initial feature image.

• To improve the results, assign some conditions such as uncorrelatedness of reduced components and linear relationships between each reduced component and the initial data.

Band Selection for Dimension Reduction in HyperSpectral Image Using Integrated Information Gain and Principal Components Analysis Technique

Kitti Koonsanit, Chuleerat Jaruskulchai, and Apisit Eiumnoh

In this paper, present band selection technique using principal components analysis (PCA) and information gain (IG) for hyper spectral image such as small multi-mission satellite (SMMS) are introduced. Band selection is an essential tool for identification of optimal spectral for different satellite applications.

Analysis of hyperspectral image is difficult due to the curse of dimensionality. So dimension reduction is an important pre-processing step in hyperspectral image analysis. The general steps involved in PCA are:

1) Find mean vector in x-space

2) Assemble covariance matrix in x-space

3) Compute Eigen values and corresponding eigenvectors

4) Form the components in y-space

In this method, the components in the direction of maximum variation are considered as first principal component. Thus only the first few components which are in the direction of maximum variation are considered.

One more technique called information gain is presented in this paper. Information gain is a measure of dependence between the feature and the class label. IG is calculated using the following formula:

$$IG(X, Y) = H(X) - H(X|Y)$$

Where H(X) is entropy of the random variable X and H (X|Y) is the entropy of band X and the entropy of band X after observing Class Y.

The maximum value of information gain is 1. Information gain is evaluated independently for each feature and the features with the top-k values are selected as the relevant features. Information Gain does not eliminate redundant features. Thus an integrated PCA and IG method is proposed. PCA and IG are integrated as:

$$\text{X Band Selected} = \text{PCA of Band} \cap \text{IG of Band}$$

The disadvantage of this method is that spatial information is not taken into account as PCA is not a spatial oriented technique.

Hyperspectral Dimension Reduction Using Global and Local Information Based Linear Discriminant Analysis

Ufuk Sakarya

In this paper complete global-local linear discriminant analysis (CGLDA) based dimension reduction of hyperspectral image is presented. This method considers both global and local pattern information for hyperspectral image processing. Unlike PCA, LDA is a supervised dimension

reduction method. This method projects data into lower dimensions in such a way that members of the same class are close to each other whereas the members of different classes are far from each other. But LDA has limitation such as the singularity problem, the distribution assumption, the small sample size problem. Moreover LDA consider global structure and ignores local structure. Thus CGLDA, which focuses on both global and local structure, is an improved version of LDA. In this paper advantages of the usage of not only global pattern information, but also local pattern information are experimentally demonstrated by comparative analysis and an experimental strategy is proposed in order to tune the parameters of CGLDA in hyperspectral application domain.

Hyperspectral data and training samples are the two inputs used in the system. There are two training processes. One of them is finding parameters of CGLDA and dimension reduction projection matrix WCGLDA. The other training is classification training. WCGLDA is used to reduce the dimension of the hyperspectral data. The classification process is applied on dimension reduced data and then classification map is obtained.

CGLDA algorithm has some drawbacks. As CGLDA is a still linear technique for feature extraction it cannot be used for applications involving non-linear relationship. The selection of balance coefficients for the proposed methods is a complex task.

Locality-Preserving Dimensionality Reduction and Classification for Hyperspectral Image Analysis

Wei Li, Saurabh Prasad, James E. Fowler, and Lori Mann Bruce

PCA and LDA assume that data are Gaussian. However, real-life observational data are often not Gaussian. In this paper, a classification method called local Fisher's discriminant analysis (LFDA) is investigated to exploit the statistical structure of the data. Local Fisher's discriminant analysis (LFDA) is used to reduce the dimensionality of HSI data and Gaussian mixture-model (GMM) classifier is employed. LFDA combines the properties of LDA and locality-preserving projections (LPP). LPP is technique that tries to find a linear map that preserves the local structure of neighbouring samples in the input space. In other words, after an LPP mapping, neighbourhood points in the original input space remain neighbours in the LPP-embedded space, and vice versa.

The spectral response of remotely sensed data can be affected by many factors, such as differences in illumination conditions, geometric features of material surfaces, and atmospheric effects. Classifiers such as those based on GMMs are hence a natural fit for remotely sensed data.

A Dimensionality Reduction Algorithm of Hyper Spectral Image Based on Fract Analysis

SU Junying, and Shu Ning

In this paper dimensionality reduction using fract analysis is described. Complex non-linear systems are analyzed using fractal method. Both spectral and spatial characteristics are considered in this method. Fractal measurement based spectral domain feature analysis for hyperspectral image has been proposed. Fractal method is widely used in remote sensing applications because of its ability to analyze both spatial structure and spatial complex. The spectral domain fractal characteristic of hyperspectral image has been emphasized by three points. First point states that spectral imaging model is a non-linear complex system. As non-linearity is the main characteristic of fractal phenomenon it is concluded that spectral curve has fractal characteristic. Second point considers the self-similar property of fractal phenomenon which states that local part of fractal is similar to whole model. The third point states that the length of spectral curve has exponential relation with band width. The methodology of fractal analysis involved three main steps: noise removal by spectral curve filtering, fractal dimension calculation of spectral curve and dimensionality reduction with the fractal dimension feature of the spectral curve.

A Robust Band Compression Technique for Hyperspectral Image Classification

Qazi Sami ul Haq,Lixin Shi,Linmi Tao,Shiqiang Yang

A dimension reduction method based on the fusion of segmented principal component analysis (SPCA) and LDA is presented in this paper. The bands are independently selected using SPCA and LDA and merged later. Fusion of SPCA and LDA preserve the properties of both algorithms: informativeness property of SPCA and information redundancy property of LDA. SPCA selects the principal components which contain the most informative features. These

components are in the direction of maximum variation. LDA tries to eliminate the shared information by maximizing the rate of between-class scatter matrix.

The constraints in the number of dimensions to be selected for SPCA and LDA are considered. For SPCA, 3 or 4 bands are found to be enough for each segment. For LDA at most c-1 dimensions are found to be available when the number of classes was c. By considering the dual criteria of informativeness and redundancy classification accuracy was improved.

Nonparametric Fuzzy Feature Extraction for Hyperspectral Image Classification

Jinn-Min Yang, Pao-Ta Yu, Bor-Chen Kuo, and Ming-Hsiang Su.

Linear discriminant analysis (LDA) is one of the most well-known methods for reducing data dimensionality in various fields. However, there are three inherent limitations when applying LDA to extract features. First, the number of features that can be extracted by LDA is the number of classes minus one at most. Second, it cannot perform well for non-normally distributed data. Third, it suffers from the singularity problem when handling the small sample size (SSS) problem. Nonparametric feature extraction algorithms such as nonparametric discriminant analysis (NDA) and nonparametric weighted feature extraction (NWFE) are developed in this paper to overcome the limitations of LDA and preserve better data structure in the reduced feature space for classification. In NFFE, fuzzification procedure is carried out and membership grades are estimated. Two remotely sensed hyperspectral image data sets are employed for testing purpose. Two classifiers are employed: 1-nearest-neighbor (1NN) and support vector machine (SVM) with RBF kernel function. The kernel function employed in SVM is RBF kernel function with a parameter σ.

Hyperspectral Image Classification and Dimensionality Reduction: An Orthogonal Subspace Projection Approach

Joseph C. Harsanyi, and Chein-I Chang

In this paper, a technique is described which simultaneously reduces the data dimensionality, suppresses undesired or interfering spectral signatures, and detects the presence of a spectral

signature of interest. The basic concept is to project each pixel vector onto a subspace which is orthogonal to the undesired signatures. This operation is an optimal interference suppression process in the least squares sense. Once the interfering signatures have been nulled, projecting the residual onto the signature of interest maximizes the signal-to-noise ratio and results in a single component image that represents a classification for the signature of interest. The orthogonal subspace projection (OSP) operator can be extended to k signatures of interest, thus reducing the dimensionality of k and classifying the hyperspectral image simultaneously. The approach is applicable to both spectrally pure as well as mixed pixels.

The technique can be viewed as a combination of two linear operators into a single classification operator. The first operator is an optimal interference rejection process in the least squares sense, and the second is an optimal detector in the maximum SNR sense. The approach is applicable to both mixed pixels as well as spectrally pure pixels, and does not suffer from the limitations of standard statistical classifiers and matched filtering/spectral signature matching techniques which are suboptimal in the presence of multiple correlated interferers.

CHAPTER 3

PRINCIPAL COMPONENT ANALYSIS AND SEGMENTED-PCA

3.1 PRINCIPAL COMPONENT ANALYSIS

Hyperspectral imaging (HSI) is one of the advanced remote sensing techniques. HSI captures data in large number of continuous spectral bands. The spectral range of HSI ranges from visible light to (near) infrared, so it is capable of detecting and identifying the minute differences of objects and their changes in temperature and moisture.

Hyperspectral image data is in the form of a hypercube. It contains 2D spatial information and 1D spectral information. Let X denotes the spatial height, Y denotes the spatial width and F denotes the spectral bands of the hypercube. Curse of dimensionality leads to a problem known as Hughes effect. HSI data is characterized by high spatial resolution (increasingly larger number of pixels per image) and spectral resolution (large number of bands). High spectral resolution implies that the classes can easily be separated, but the number of statistical parameters defining the class increases. As the training sample available for remote sensing data is limited classification accuracy decreases.

Thus it is difficult to work with high dimensional data. Consequently, effective feature extraction and data reduction is required. Due to the high redundancy between neighbouring spectral bands, such data reduction is feasible. Principal component analysis (PCA) is the most widely used method for this purpose. PCA transform the original coordinate system into new orthogonal coordinate system to convert high dimensional data into linearly uncorrelated variables, namely principal components. The first principal component is in the direction of maximum variation, second component is in the direction of next maximum variation and so on. Thus by considering only the first few principal components the data can be projected into lower dimensional space. PCA and its variants called Segmented-PCA (Seg-PCA) and Folded-PCA (F-PCA) has been implemented and a comparative analysis of the three methods is carried out.

Principal component analysis (PCA) is widely used linear dimensionality reduction technique. Band selection is an essential tool for identification of optimal spectral for different

satellite applications. Analysis of hyperspectral image is difficult due to the curse of dimensionality. So dimension reduction is an important pre-processing step in hyperspectral image analysis. The general steps involved in PCA are:

1) Find mean vector in x-space

2) Find covariance matrix in x-space

3) Compute Eigen values and corresponding eigenvectors

4) Form the components in y-space

In this method, the components in the direction of maximum variation are considered as principal components. Thus only first few components contain the needed information. Fig.3.1 shows the PCA approach to dimensionality reduction. Conventional PCA has high computational cost, large memory requirement and low efficacy when dealing with high dimensional data.

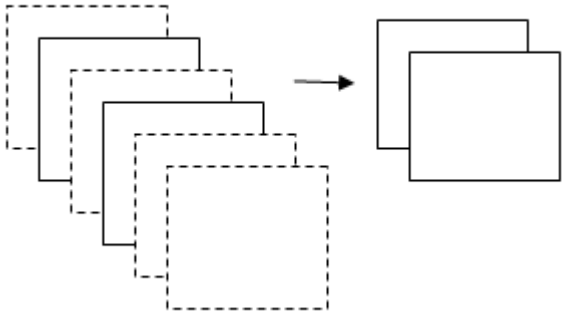

Figure.3.1 PCA dimension reduction technique

Let the spectral vector in a hypercube be represented as $X_n = [X_{n1}, X_{n2}, \dots X_{nF}]^T$. The value of n ranges from 1 to S, where S is the spatial size of the image cube and F is the number of spectral bands. The hypercube is converted to matrix of size F x S in conventional PCA. Next step is to obtain mean adjusted spectral vector as follows

$$I_n = X_n - \bar{I} \qquad (1)$$

$$\bar{I} = \frac{1}{S} \sum_{n=1}^{S} X_n \qquad (2)$$

Let $I_0 = [I_1, I_2, \ldots . I_F]$ be a matrix formed by these mean adjusted vectors. Then the covariance matrix C is obtained as

$$C = E\{(X_n - E\{X_n\})(X_n - E\{X_n\})^T\} \quad (3)$$

where E {.} denotes the mathematical expectation. Calculation of C usually causes memory overflow problems as matrix I_0 has large dimension.

The covariance matrix can be approximated as:

$$C_x = \frac{1}{S}\sum(X_n - \bar{I})(X_n - \bar{I})^T \quad (4)$$

The PCA is based on the Eigen value decomposition of the covariance matrix, which takes the form of:

$$C_x = ADA^T \quad (5)$$

Where D=diag ($\lambda_1, \lambda_2 \ldots \lambda_F$) is the diagonal matrix composed of the Eigen values $\lambda_1, \lambda_2 \ldots \lambda_F$ of the covariance matrix C_x, and A is the orthonormal matrix composed of the corresponding F dimension Eigen vectors a_k of C_x as follows:

$$A = [a_1, a_2, \ldots a_F] \quad (6)$$

The linear transformation defined by:

$$y_n = A^T X_n \quad (7)$$

The data projection results in:

$$z_n = [z_{n1}, z_{n2}, \ldots z_{nk}]^T \quad (8)$$

3.2 SEGMENTED-PCA

In segmented-PCA, each spectral vector of F bands is grouped into small vectors and PCA is calculated for each group. Let the spectral vector is segmented to H subgroups, each group containing W bands. For a particular group, $b \in [1, H]$ let $I_{mb} = \left[I_{1m}, I_{2m}, \ldots I_{n_b m}\right]$ represents the small spectral vector, where $m = [1, S]$ and C_b the covariance matrix. Then C_b can be determined as follows

$$C_b = \frac{1}{S}\sum_{m=1}^{S} I_{mb} {I_{mb}}^T \qquad (9)$$

Here $I_{mb} {I_{mb}}^T$ denotes the partial covariance matrix obtained from the grouped spectral vector I_{mb}. Thus conventional PCA extracts principal components from the whole F bands while segmented PCA groups the spectral vector into H groups and extracts the local structures.

Fig.3.2 shows the multistage segmented PCA process schematically. The complete data set is first partitioned into subgroups. Highly correlated bands are selected as subgroups. The number of bands in subgroups $1,2,..k$ is denoted by $n_1, n_2, ... n_k,$ respectively. The principal component transformation is conducted separately on each subgroup of data.

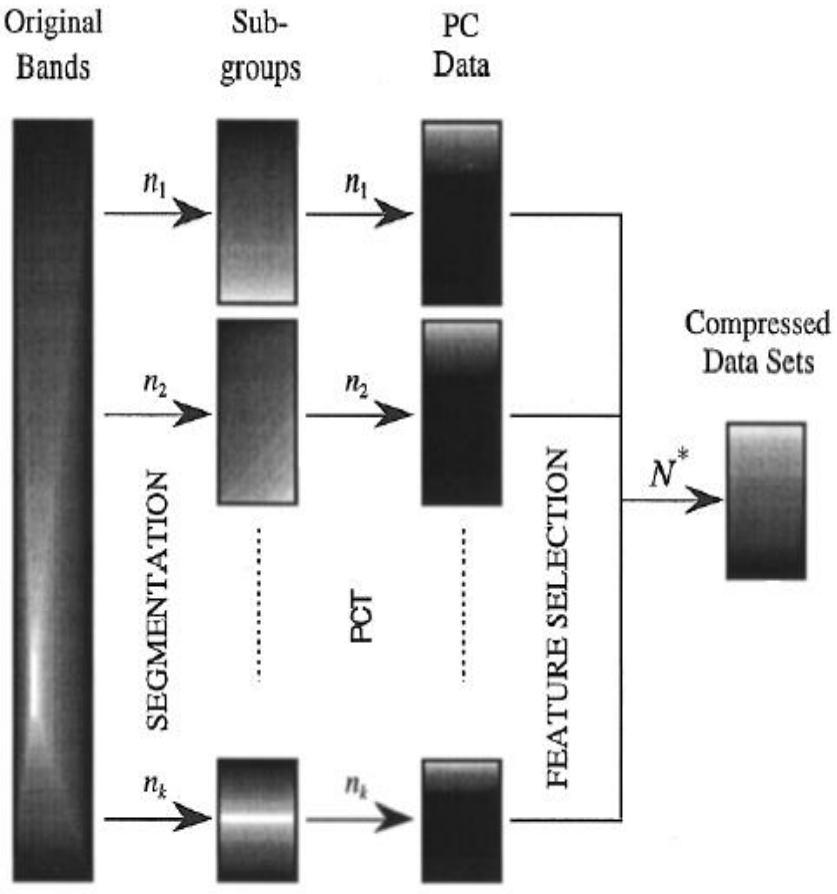

Figure.3.2 Schematic chart of Segmented-PCA

In one particular case where all groups contain the same number of W bands, $HW = F$, the covariance matrices from different groups share the same dimension. As a result, they can be summed to form one covariance matrix. This can further simplify the Eigen-decomposition procedure for better efficiency, as only one matrix rather than k must be processed.

CHAPTER 4

FOLDED-PCA

In folded-PCA, the covariance matrix is obtained by accumulation of S partial covariance matrices, which are obtained from a much smaller matrix formed by folding the featured F bands into a matrix. As each spectral vector is represented in the form of a matrix, correlation between bands and band groups are successfully extracted in calculating the partial covariance matrix. To this end, improved results with reduced computational burden on data reduction and feature extraction are achieved.

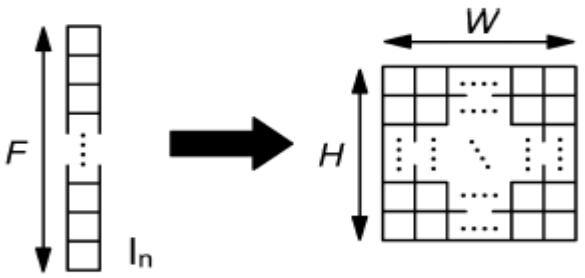

Figure.4.1 Construction of a 2D matrix by folding a 1D spectral vector.

The matrix representation of each spectral vector is shown in the Fig.4.1. Here the whole F bands are folded into H groups or segments and each row of the matrix contains a group of W bands. When $H = 1$, Folded-PCA degrades to the conventional PCA. The performance of the Folded-PCA is dependent to the selected H, as it affects how much additional information can be extracted for added-value to the conventional PCA. From this matrix-based representation, the obtained covariance matrix helps to extract not only global structure but also local structures hence it is superior to conventional PCA.

For a spectral vector $I_n = [I_{n1}, I_{n2}, \dots I_{nF}]^T$ let A_n is the $H \times W$ matrix obtained. We have

$$A_n = \begin{bmatrix} a_{n1} \\ \vdots \\ a_{nH} \end{bmatrix} \tag{10}$$

$$a_{nh} = \left[I_{n(1+W(h-1))}, \ldots . I_{n(W+W(h-1))}\right] \quad (11)$$

Where $h \in [1, H]$

Next step is to calculate the partial covariance matrix of $\mathbf{A}_n$. This is obtained as follows:

$$C_n = {A_n}^T A_n \quad (12)$$

Finally, the overall covariance matrix for the whole hypercube is determined as the accumulation of these partial covariance matrices as follows

$$C_{F-PCA} = \frac{1}{S} \sum C_n \quad (13)$$

The Eigen problem is to decompose the covariance matrix into the multiplication of three matrices, i.e. orthonormal matrix, diagonal matrix D and ${A_n}^T$. Diagonal matrix contains the Eigen values of the covariance matrix and orthonormal matrix is composed of the corresponding Eigen vectors. The covariance matrix C_{F-PCA} is of size $W \times W$ while the covariance matrix from conventional PCA is of size $F \times F$. As a result, the computational costs for the Eigen problem in our Folded-PCA have been significantly reduced.

Eventually, data projection is to done. For the covariance matrix C_{F-PCA}, let q' be the number of selected Eigen values and α the matrix formed using Eigen vectors for data projection. For each row vector in A_n, q' components are extracted by multiplying it with α which results in $q = Hq'$ features extracted for the whole sample. Thus the data obtained from projection is determined by multiplying two smaller matrices as follows, which has also significantly reduced the computational cost.

$$z_n = A_n \alpha \quad (14)$$

The advantages of using the proposed Folded-PCA are summarized as follows.

- Improved discrimination capability as in Folded-PCA the matrix-like analysis enables extraction of local structure from the hypercube spectral domain. This is achieved by extracting features from each grouped bands, i.e. the row vectors in A_n to ensure local features within these band groups are covered.
- Significantly reduced complexity of the overall algorithm due to a much smaller covariance matrix being required.

- Reduced memory usage in determining the covariance matrix and subsequent analysis.

The covariance matrices of all the three methods are shown in Fig.4.2. Memory requirement for the covariance matrix computation is high for PCA in comparison to Seg-PCA and F-PCA.

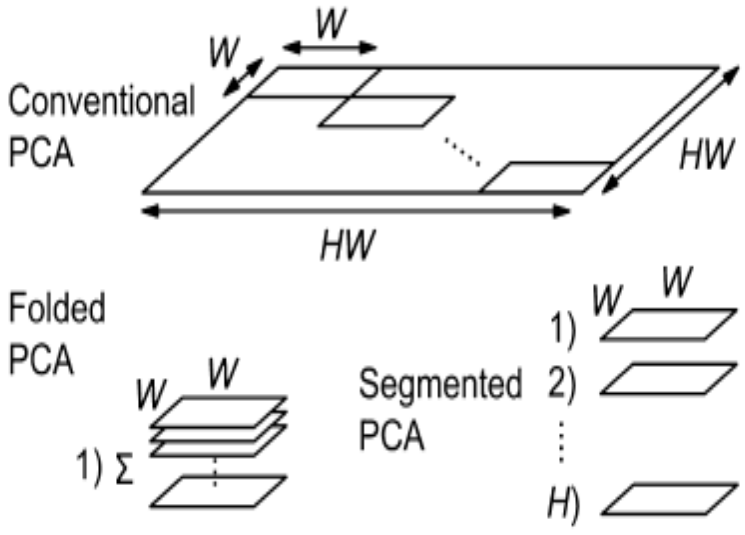

Figure.4.2 Covariance matrix comparison for three different PCA schemes, i.e. conventional PCA , Folded-PCA and Segmented PCA.

The covariance matrix of PCA is of size F x F. But in Seg-PCA, there is W number of covariance matrices. In F-PCA, the size of covariance matrix is W x W.

4.1 F-PCA IMPLEMENTATION

The implementation of F-PCA with stopping rule and noise removal is shown in Fig.4.3. Four Hyperspectral images are used for the study. The total number of bands is denoted as F. Each spectral vector is folded into a matrix of size $H \times W$. Mean is calculated for each column and subtracted from the pixel values. The covariance matrix is obtained for the folded matrices. The partial covariance matrices so obtained are combined to obtain the covariance matrix of size $W \times$ W. The Eigen values and Eigen vectors are obtained by the singular value decomposition (SVD) of the covariance matrix.

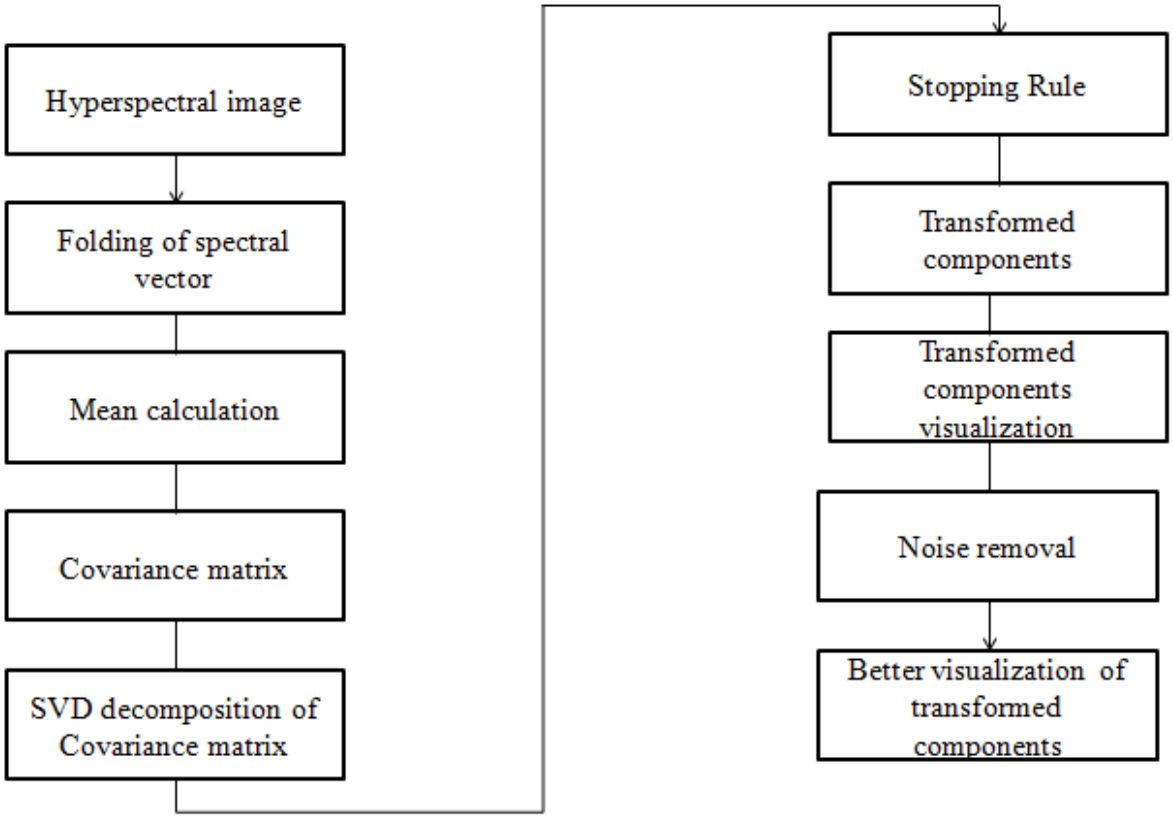

Figure.4.3 F-PCA implementation with stopping rule and noise removal

4.1.1 Intrinsic Dimensionality

Selecting the optimum number of transformed bands for obtaining the dimensionality reduced image is real task, as there are no standards to calculate them. After the reduced bands of the complete hyperspectral image are obtained and their variability are calculated here comes the important part where the number of bands are to be selected. This process of selecting optimum bands where most of the data is contained is known as intrinsic dimensionality of the image. A ststistical method has been developed by calculating the number of bands falling into the threshold set on the percentage variability of the image. This threshold is set as 98-99 % of variability.

4.1.2 Noise Removal

The amount of noise included in a hyperspectral image makes its analysis difficult. The existence of noise in a hyperspectral image not only influences the visual effect of these images but also limits the precision of the subsequent processing. Therefore, it is critical to reduce the noise in the hyperspectral image and improve its quality. Median filter is used here to eliminate the noise.

Spatial median filters work by decreasing the variance within a small window (kernel) by assigning a pixel the median value of the surrounding pixels. For example, using a 3 × 3 window, a median filter would assign a pixel the median value of itself and its eight immediate neighbors (top, left, right, bottom, and four diagonal locations). As geographic data is highly correlated, the variance of the signal within such a window should be small, and noise should be random and not correlated within a neighborhood, making a large variance probable. With the assumption that the variance of the noise is larger than that of the signal in these small windows, a spatial filter such as a median filter will preserve most of the signal while eliminating much of the noise. A filter with a larger window has a more dramatic smoothing effect over a filter with a small window, resulting in a larger SNR at the expense of the signal. A median filter has the property of preserving original values unlike a mean filter. The work flow of median filter is shown in Fig.4.4

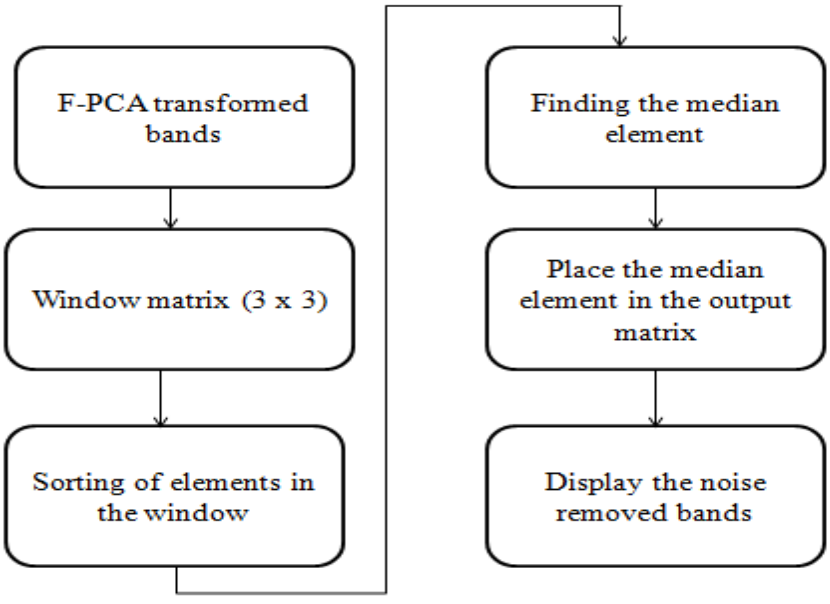

Figure.4.4 Noise removal flowchart

A 2D image of size m x n is input to the filter. Then another matrix of size (m+2 by n+2) is preallocated with zeros. The input matrix is copied to the preallocated matrix. A window matrix of size 3 x 3 is formed with elements of input matrix. Then the window matrix is copied into an array and it is sorted. The median element is found out . Here it is 5th element. (The total elements are 9. The middle element will be 5). The fifth element is placed into the output matrix. The procedure is repeated for complete input matrix and the image is displayed without noise.

4.1.3 Methodology for Comparison

The overall methodology is shown in Fig.4.5. Hyperspectral images are taken and dimensionality reduction is carried out using existing techniques such as PCA and Segmented-PCA and proposed method F-PCA. F-PCA has been implemented with stopping rule and noise removal.

The transformed bands obtained by all the three methods are analysed for comparative study. The parameters used are Peak Signal to Noise Ratio (PSNR), Structural Similarity Index (SSIM), computational time and memory requirement.

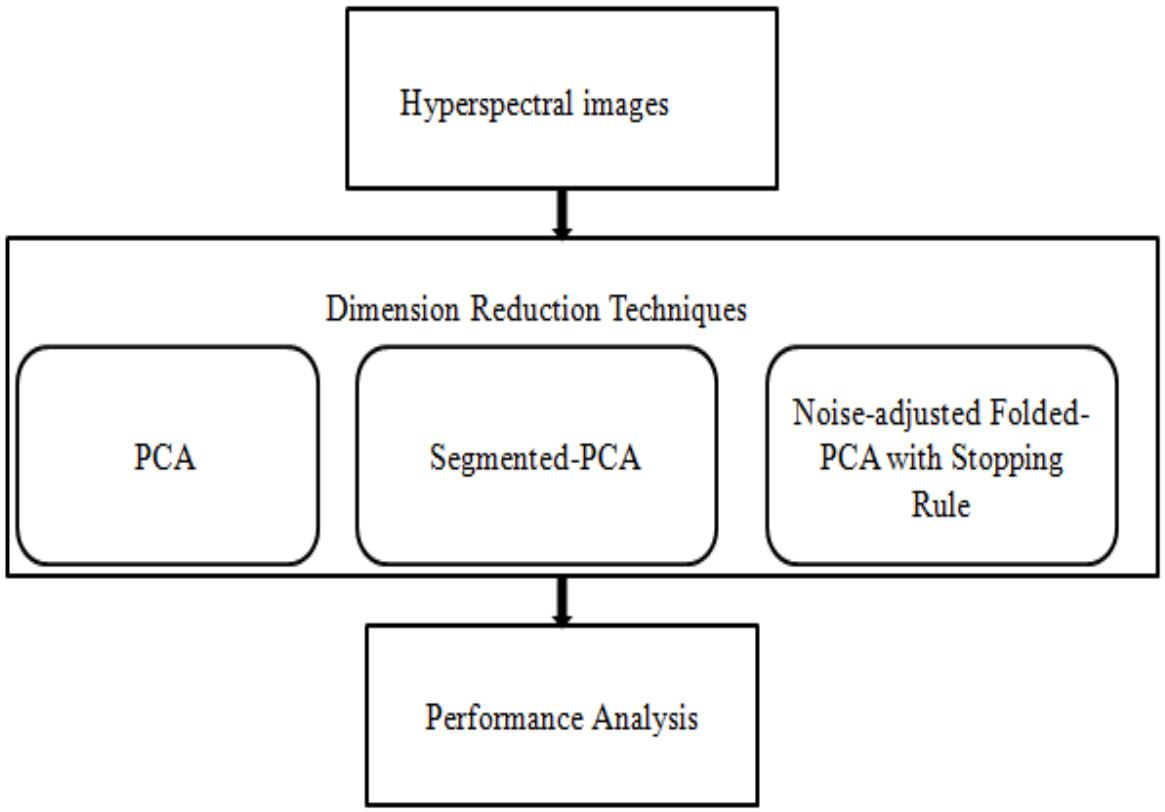

Figure 4.5 Methodology for comparison of all the three techniques

4.1.4 Parameters Used for Comparison

- **Peak Signal to Noise Ratio (PSNR):**

Peak signal-to-noise ratio, often abbreviated PSNR, is an engineering term for the ratio between the maximum possible power of a signal and the power of corrupting noise that affects the fidelity of its representation. Because many signals have a very wide dynamic range, PSNR is usually expressed in terms of the logarithmic decibel scale.

PSNR is most commonly used to measure the quality of reconstruction of lossy compression codecs (e.g., for image compression). The signal in this case is the original data, and the noise is the error introduced by compression. PSNR is given by:

$$PSNR = 20log\frac{Max_i}{\sqrt{MSE}} \qquad (15)$$

Here Max_i is the maximum pixel value of the image.

- **Structural Similarity Index (SSIM):**

The structural similarity (SSIM) index is a method for measuring the similarity between two images. The SSIM index is a full reference metric; in other words, the measuring of image quality based on an initial uncompressed or distortion-free image as reference. The difference with respect to other techniques mentioned previously such as MSE or PSNR is that these approaches estimate perceived errors; on the other hand, SSIM considers image degradation as perceived change in structural information.

Structural information is the idea that the pixels have strong inter-dependencies especially when they are spatially close. These dependencies carry important information about the structure of the objects in the visual scene. The measure between two windows x and y of common size N x N is:

$$\text{SSIM} = \frac{(2\mu_x\mu_y+c_1)(2\sigma_{xy}+c_2)}{(\mu_x{}^2+\mu_y{}^2+c_1)(\sigma_x{}^2+\sigma_y{}^2+c_2)} \qquad (16)$$

With

- μ_x the average of x
- μ_y the average of y
- $\sigma_x{}^2$ the variance of x
- $\sigma_y{}^2$ the variance of y
- σ_{xy} the covariance of x and y
- c_1 and c_2 two variables to stabilize the division with weak denominator

Other parameters used for comparison are memory requirement and computation time. Memory requirement is calculated based on the data matrix and covariance matrix size. The saving factor is determined based on the memory requirement comparison.

CHAPTER 5

SIMULATION RESULTS

5.1 HYPERSPECTRAL IMAGES

Four hyperspectral images are used for study. MATLAB software is used for simulation. First three images are the Hyperion image of Lake Monona, Erta Ale, and Mt. St. Helens. These images are provided by the EO-1 Mission, NASA/USGS. The number of spectral channels is 242. The samples are stored as 2-byte unsigned integer and arranged in BIP order. The fourth image is Airborne Visible/Infrared Imaging Spectrometer (AVIRIS) image of Moffett Field. The entire image contains 614 samples, 224 bands and each sample is stored as 16-bit signed integers. These data are made available on JPL's website. The details of hyperspectral data sets are given in table 5.1.

Table 5.1 Hyperspectral data sets

Image Name	**Sensor Name**	**Spatial Size**	**Number of Bands**
Lake Monona	Hyperion	317 x 256	242
Erta Ale	Hyperion	317 x 256	242
Mt. St. Helens	Hyperion	324 x 256	242
Moffett Field	AVIRIS	317 x 614	224

One band image of Lake Monona, Erta Ale, Mt. St. Helens and Moffett Field are shown in Figs.5.1(a), (b), (c) and (d), respectively.

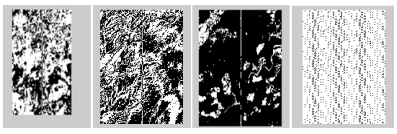

(a) (b) (c) (d)

Figure.5.1 One band image (a) Lake Monona (b) Erta Ale (c) Mt. St. Helens (d) Moffett Field

Quick look images of all the four data sets are shown in Figs.5.2 (a), (b), (c) and (d). Lake Monona is a freshwater drainage lake in Dane County, Wisconsin surrounded on three sides by the city of Madison, Wisconsin and on the south side by the city of Monona, Wisconsin. It is the second-largest of a chain of four lakes along the Yahara River (also including Mendota, Kegonsa, and Waubesa) in the area and forms the south shore of the isthmus that forms downtown Madison.

Erta Ale (or Ertale or Irta'ale) is a continuously active basaltic shield volcano in the Afar Region of northeastern Ethiopia. It is situated in the Afar Depression, a badland desert area spanning the border with Eritrea. Erta Ale is the most active volcano in Ethiopia.

Mount St. Helens (known as Lawetlat'la to the indigenous Cowlitz people and Loowit to the Klickitat) is an active stratovolcano located in Skamania County, Washington, in the Pacific Northwest region of the United States. It is 96 miles (154 km) south of Seattle, Washington, and 50 miles (80 km) northeast of Portland, Oregon. Mount St. Helens takes its English name from the British diplomat Lord St Helens, a friend of explorer George Vancouver who made a survey of the area in the late 18th century. The volcano is located in the Cascade Range and is part of the Cascade Volcanic Arc, a segment of the Pacific Ring of Fire that includes over 160 active volcanoes. This volcano is well known for its ash explosions and pyroclastic flows.

Moffett Federal Airfield, also known as Moffett Field, is a joint civil-military airport located between southern Mountain View and northern Sunnyvale, California, USA. The airport is near the south end of San Francisco Bay, northwest of San Jose. Formerly a United States Navy facility, the former naval air station is now owned and operated by the NASA Ames Research Centre. Tenant military activities include the 129th Rescue Wing of the California Air National Guard, operating the MC-130P Combat Shadow and HH-60G Pave Hawk aircraft, as well as the adjacent Headquarters for the 7th Psychological Operations Group of the U.S. Army Reserve. Until 28 July 2010, the U.S. Air Force's 21st Space Operations Squadron was also a tenant command at Moffett Field, occupying the former Onizuka Air Force Station. In addition to these military activities, NASA also operates several of its own aircraft from Moffett.

(a) Lake Monona

(b) Erta Ale

(c) Mt.St. Helens

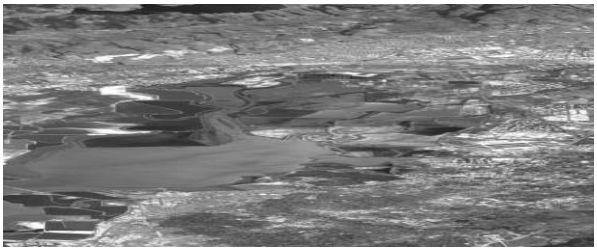

(d) Moffett Field

Figure.5.2 Quick look images

5.2 F-PCA IMPLEMENTATION RESULTS

The folding optimization is carried out in F-PCA based on the PSNR valued obtained for different folding. For all the test images it was found that the optimum value is obtained when the difference between H and W is minimum. The folding optimization table is given below. The optimum values are highlighted.

Table 5.2 PSNR values for different folding

Image Name	***H***	***W***	**Average PSNR (dB)**
Lake Monona	2	121	36.41
	11	**22**	**58.94**
Erta Ale	2	121	36.07
	11	**22**	**56.97**
Mt. St. Helens	2	121	39.67
	11	**22**	**59.69**
Moffett Field	2	112	7.59
	4	56	15.89
	7	32	27.75
	8	28	31.70
	14	**16**	**44.06**

The variance plot for all the four images for different number of components is shown in Fig.5.3. The threshold is set to be 98-99 % of the cumulative variance. For Lake Monona the number of components to be retained is 20. For Erta Ale and Mt.St.Helens, 19 components are to be retained. In the case of Moffett Field, 6 components contribute 98-99% of the cumulative variance.

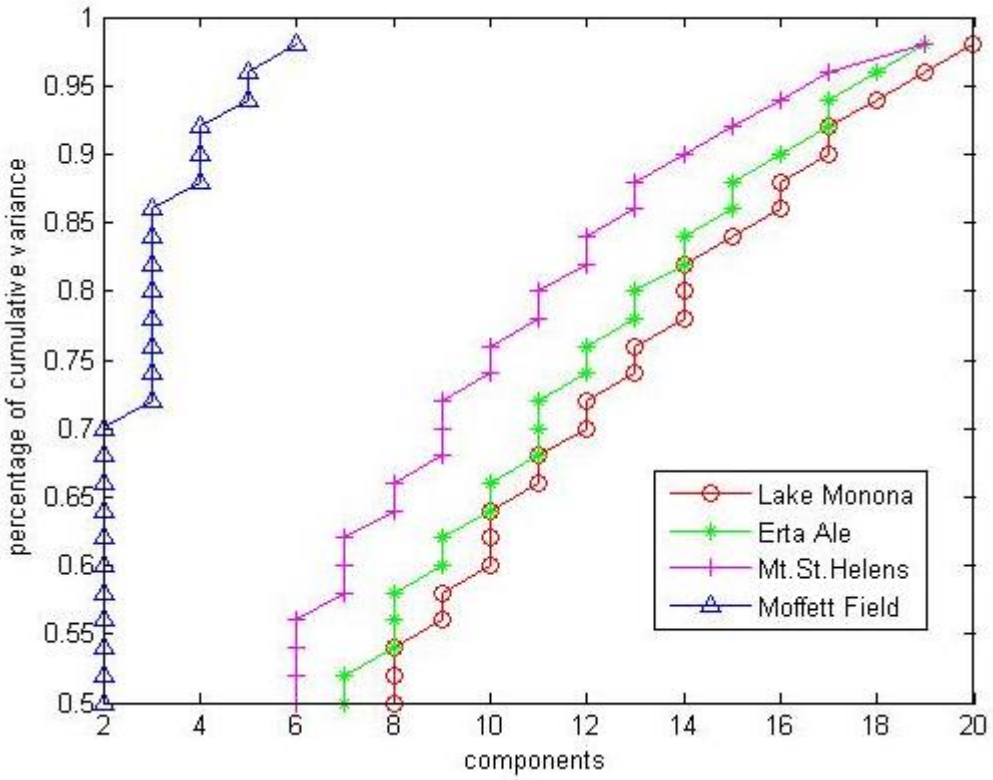

Figure.5.3 Variance plot of various number of components

The results of noise removal are shown in Figs.5.4 through 5.7. As can be seen the images are better visualised after the noise removal.

(a) With noise

(b) Without noise

(c) With noise

(d) Without noise

Figure.5.4 Lake Monona images with and without noise

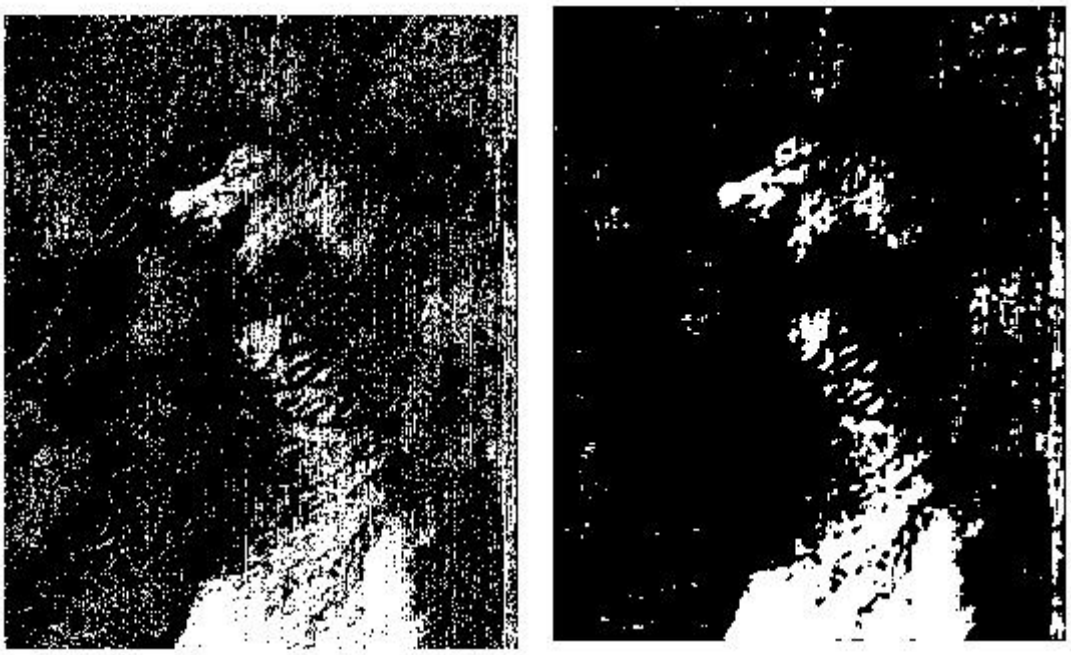

(a) With noise

(b) Without noise

(c) With noise

(d) Without noise

Figure.5.5.Erta Ale images with and without noise

(a) With noise

(b) Without noise

(c) With noise

(d) Without noise

Figure.5.6. Mt.St.Helens images with and without noise

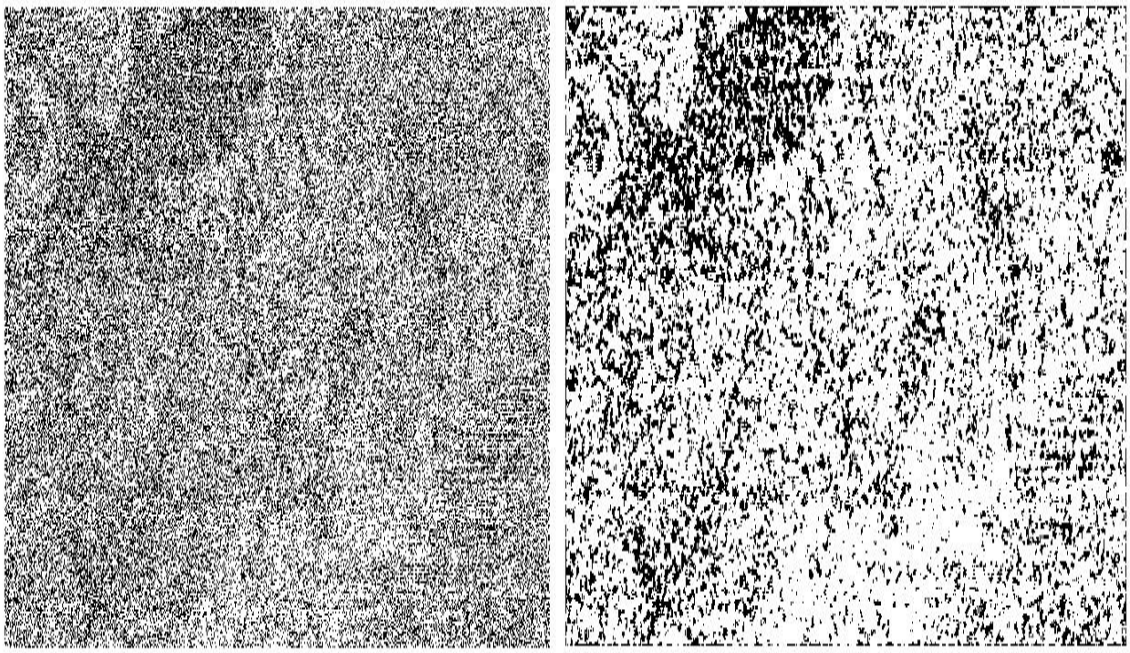

(a) With noise (b) Without noise

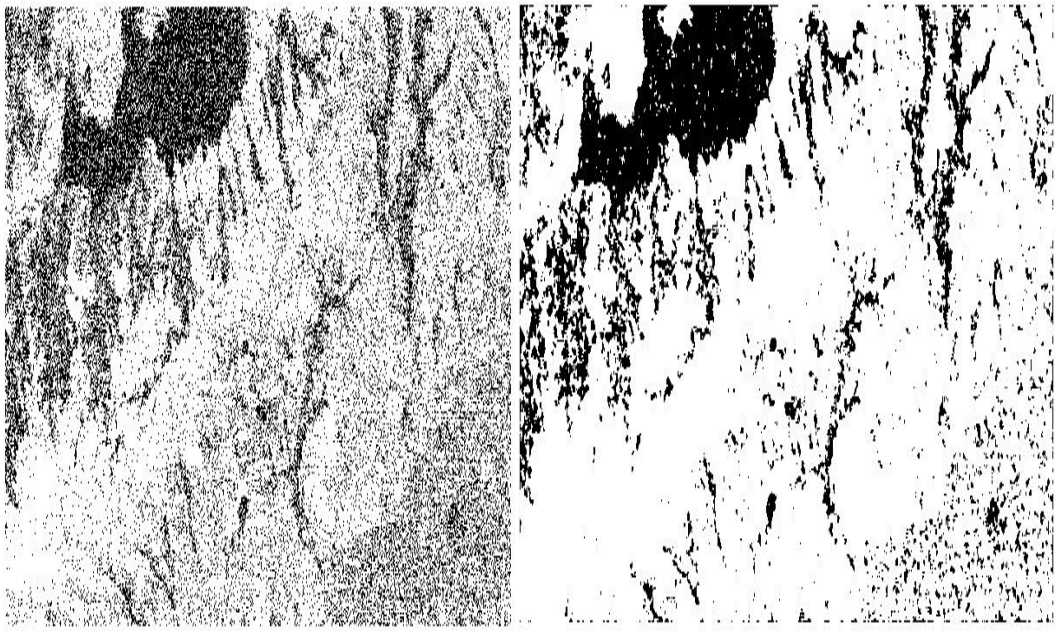

(c)With noise (d) Without noise

Figure.5.7 Moffett Field images with and without noise

5.3 COMPARATIVE STUDY OF PCA, Seg-PCA and F-PCA

The covariance matrix obtained for Lake Monona and Moffett -Field image using PCA, Seg-PCA and F-PCA are shown in Figs.5.8 and 5.9, respectively.

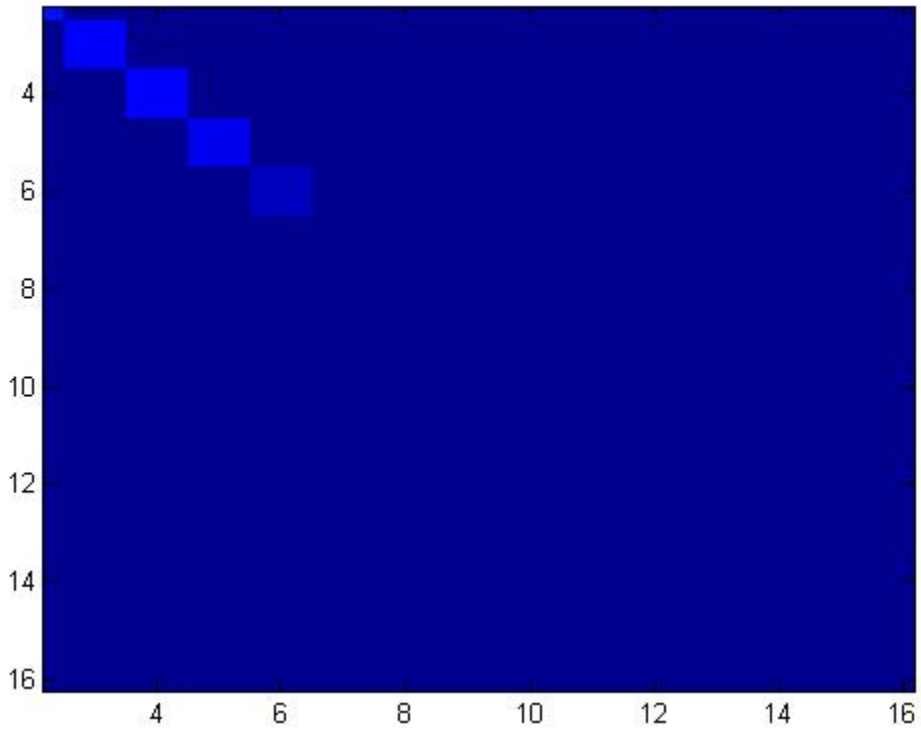

(a)

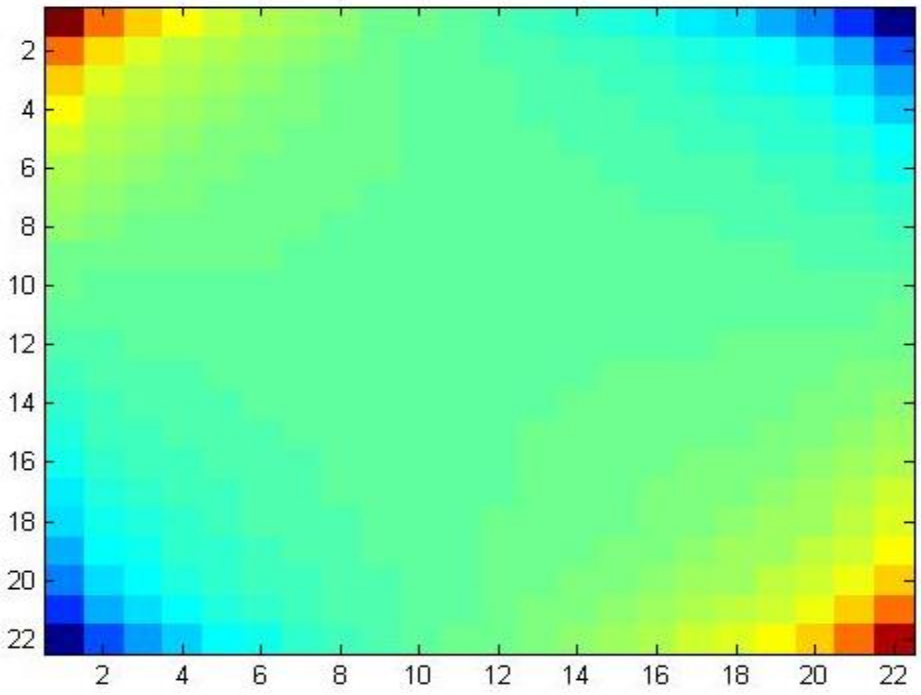

(b)

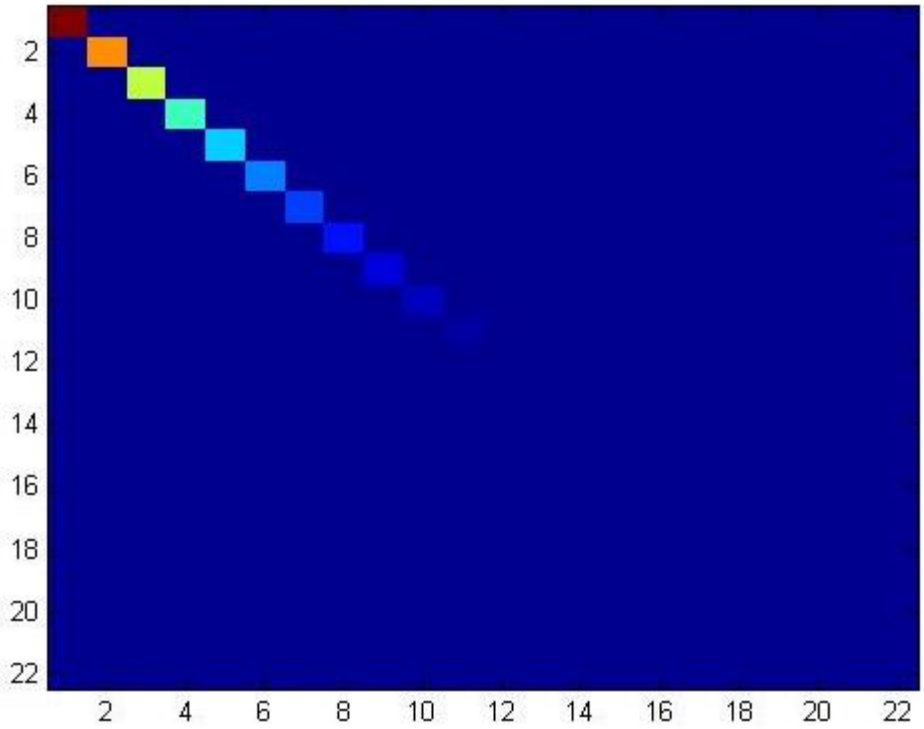

(c)

Figure.5.8 Covariance matrix of Lake Monona by (a) PCA (b) Seg-PCA and (c) F-PCA method

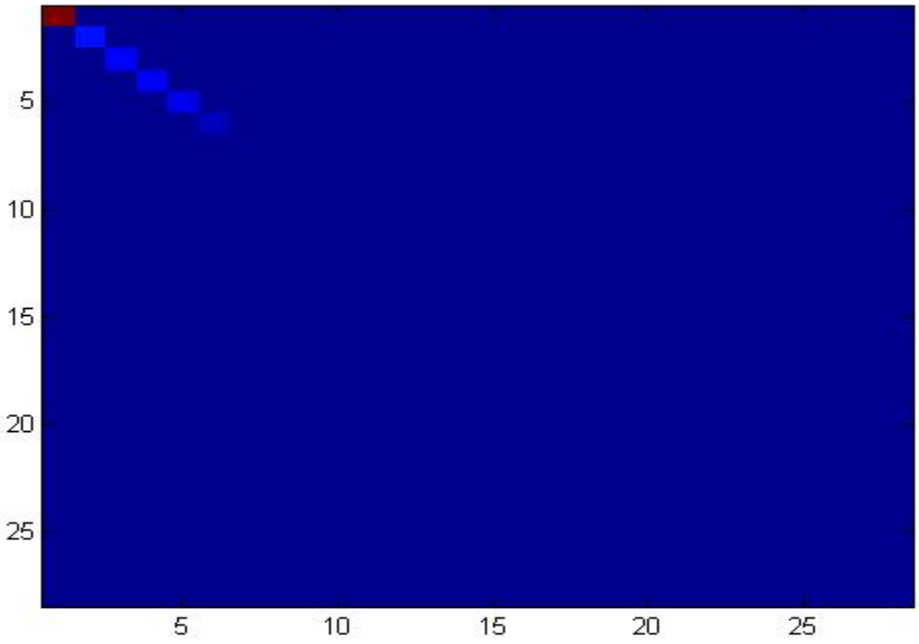

(a)

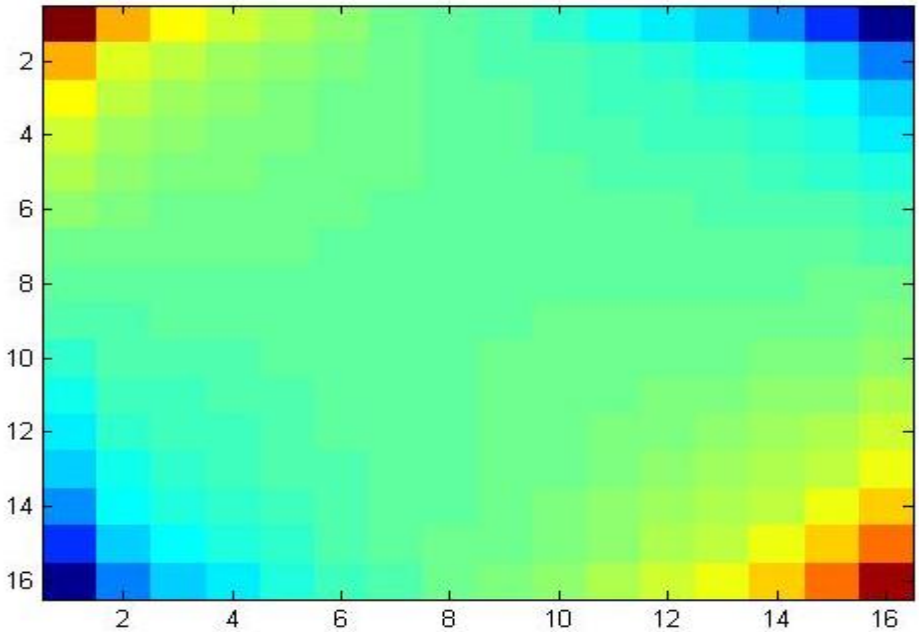

(b)

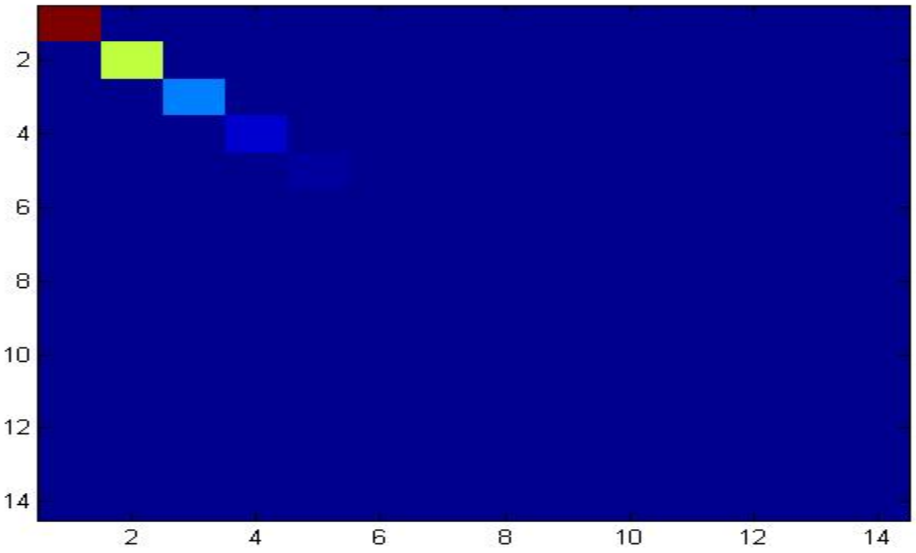

(c)

Figure.5.9 Covariance matrix of Moffett-Field by (a) PCA (b) Seg-PCA and (c) F-PCA method

The data matrix and covariance matrix size in all the three methods is tabulated below. As can be seen, the size of PCA covariance matrix is F×F always. But F-PCA and Seg-PCA has covariance matrix of size W×W. Thus there is a saving factor of H^2.

Table 5.3 Memory requirement

Method	**Stage**	
	Data matrix	**Covariance matrix**
PCA	S x HW	HW x HW
Seg-PCA	H x W	W xW
F-PCA	H x W	W xW

The proposed F-PCA method is compared with PCA and Seg-PCA in terms of PSNR, SSIM and computation time also. The images obtained by all the three methods for each images is shown

in Figs.5.9 through 5.12. It is obvious that F-PCA has better visualization in comparison to PCA and Seg-PCA.

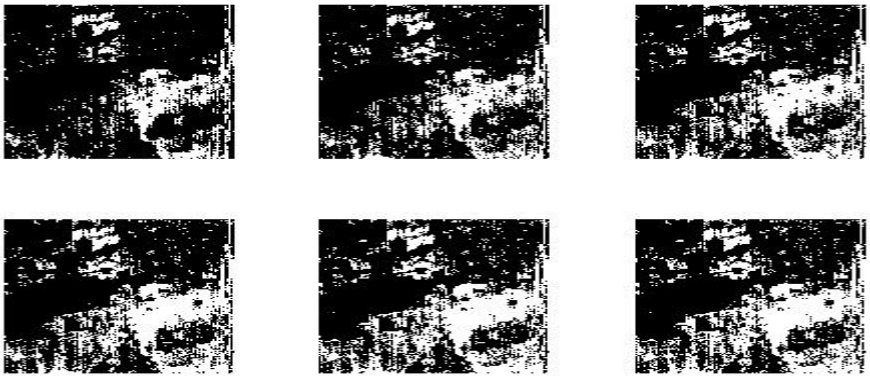

(a) PCA

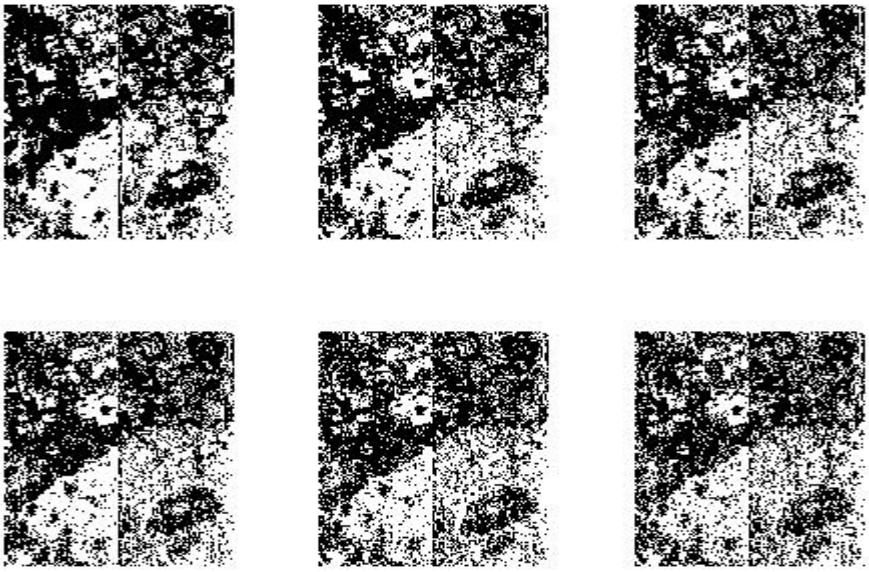

(b) Seg-PCA

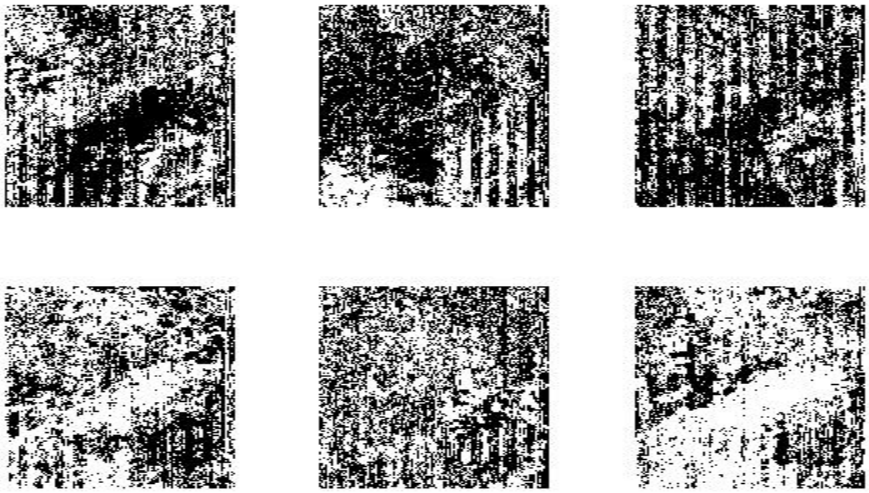

(c) F-PCA

Figure.5.10 Spatial scenes obtained for Lake Monona

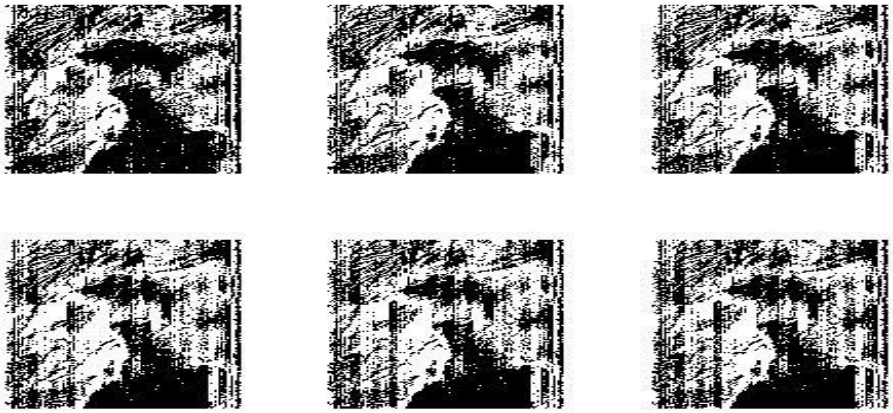

(a) PCA

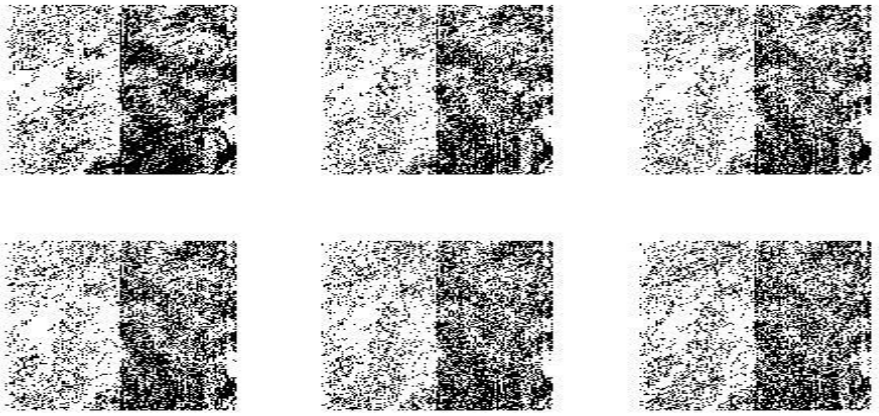

(b) Seg-PCA

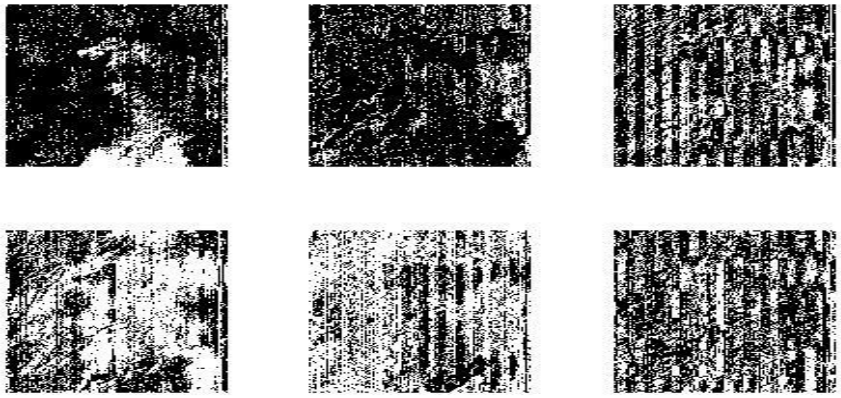

(c) F-PCA

Figure.5.11. Spatial scenes obtained for Erta Ale

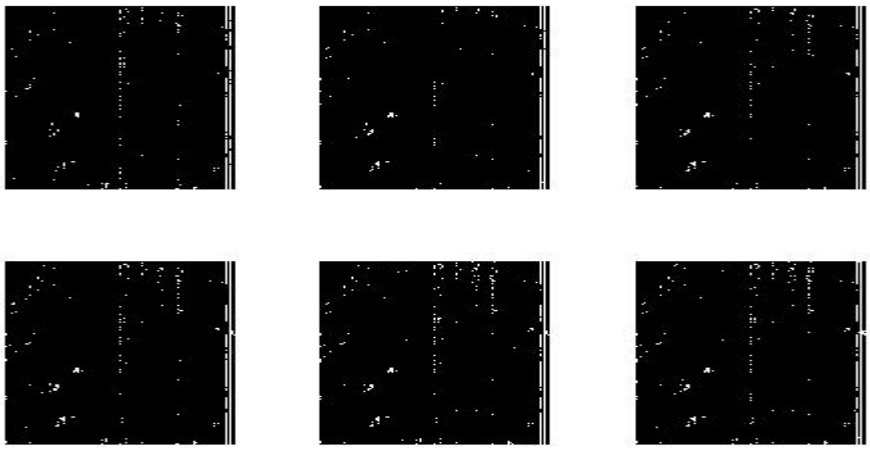

(a) PCA

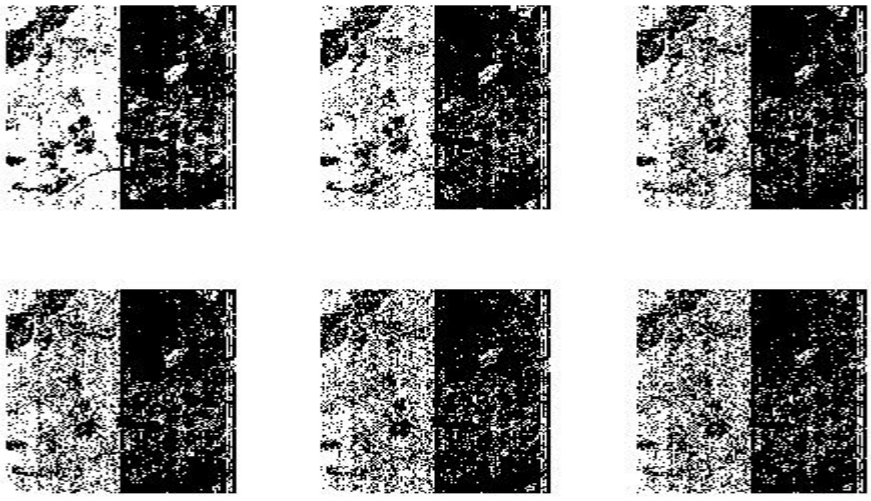

(b) Seg-PCA

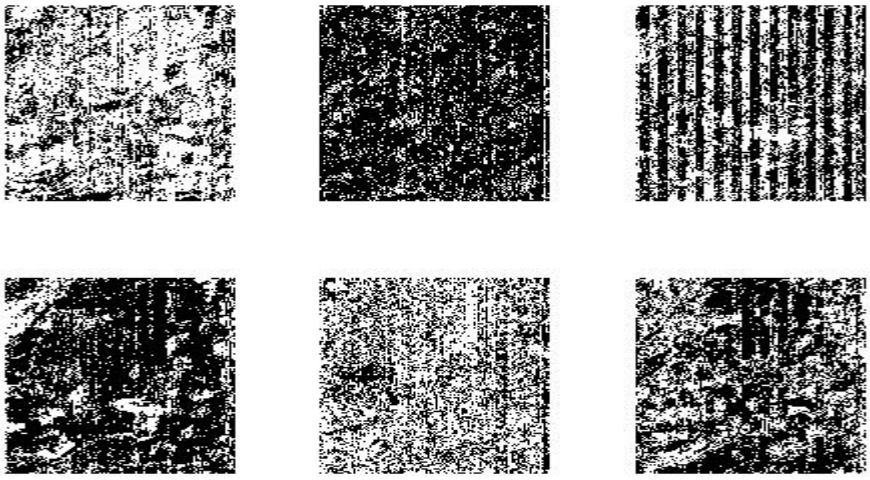

(c) F-PCA

Figure.5.12. Spatial scenes obtained for Mt.St.Helens

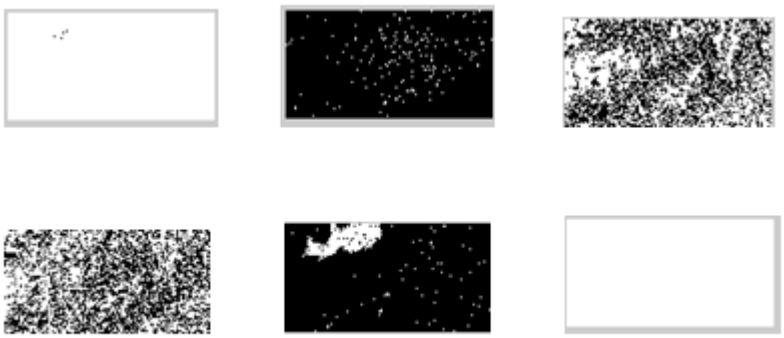

(a) PCA

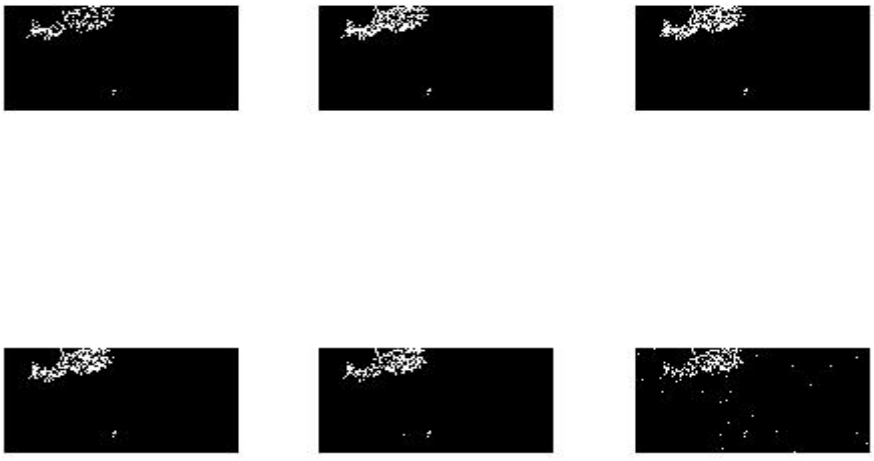

(b) Seg-PCA

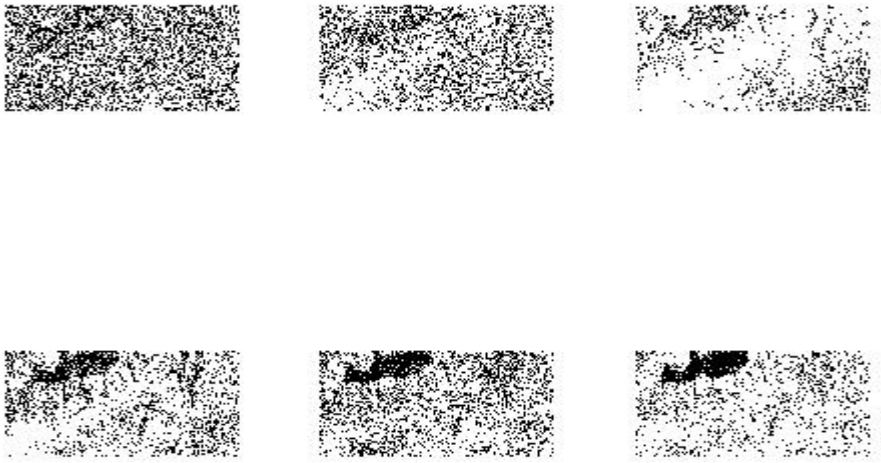

(c) F-PCA

Figure.5.13. Spatial scenes obtained for Moffett Field

The numerical values of PSNR, SSIM and time for each of the images are given in table 5.4 through 5.7. F-PCA has high PSNR and SSIM values in comparison to PCA and Seg-PCA. Memory requirement of F-PCA and Seg-PCA is same, and computation time of F-PCA is less.

Table 5.4 Comparison table for Lake Monona

Method	**Parameters**		
	Average PSNR (dB)	**Average SSIM**	**Computation Time (sec)**
PCA	27.00	0.8227	117.87
Seg-PCA	50.27	0.9158	226.64
F-PCA	58.12	0.9405	30.2

Table 5.5 Comparison table for Erta Ale

Method	**Parameters**		
	Average PSNR (dB)	**Average SSIM**	**Computation Time (sec)**
PCA	29.02	0.8591	110.1
Seg-PCA	42.83	0.9075	248.8
F-PCA	56.97	0.9344	24.2

Table 5.6 Comparison table for Mt.St.Helens

Method	**Parameters**		
	Average PSNR (dB)	**Average SSIM**	**Computation Time (sec)**
PCA	26.18	0.8090	120.01
Seg-PCA	44.85	0.9009	228.84
F-PCA	59.80	0.9298	31.81

Table 5.7 Comparison table for Moffett Field

Method	Parameters		
	Average PSNR (dB)	**Average SSIM**	**Computation Time (sec)**
PCA	29.65	0.8497	241.22
Seg-PCA	33.69	0.8999	289.47
F-PCA	39.12	0.9290	36.54

The Hyperion and AVIRIS sensors are compared in terms of PSNR in table. Both images have almost same PSNR for PCA method. Image captured by Hyperion sensor has high PSNR for Seg-PCA and F-PCA method.

Table 5.8 Comparison of Hyperion sensor and AVIRIS sensor images

Method	**PCA**	**Seg-PCA**	**F-PCA**
Lake Monona	28.43	51.76	58.94
Moffett Field	28.35	41.61	44.06

CHAPTER 6

CONCLUSION AND FUTURE WORK

Dimensionality reduction of hyperspectral image has been carried out using Folded-PCA with stopping rule and noise removal. Although PCA has been widely used for data reduction, it suffers from three main drawbacks, i.e. extremely high computational cost, large memory requirement and low efficacy in processing large dimensional datasets such as HSI. Proposed Folded-PCA approach, successfully resolves these drawbacks, where the computational cost is reduced by one order of magnitude. Since the proposed Folded-PCA approach can extract not only a global structure but also local structures within the dataset, it provides real added-value to the data analysis. The main characteristic of F-PCA is the way it folds the spectral vector for efficient calculation of covariance matrix. This leads to the efficient extraction of features. With a PCA-style analysis, the proposed Folded-PCA has proved to be both efficient and effective in data reduction.

The proposed method is compared with PCA and Seg-PCA in terms of PSNR, SSIM, memory requirement and time. F-PCA is found to be having high value for PSNR and SSIM. The memory requirement of F-PCA and Seg-PCA are same and it is less than that of PCA. The computation time of F-PCA is less compared to the other two methods.

As a future work classification using Support Vector Machine (SVM) can be implemented. The features extracted using PCA, Seg-PCA and F-PCA is fed to a standard SVM for comparisons. The overall classification accuracy is taken as an objective measurement for quantitative evaluation. The reasons to choose SVM are not only that it exploits a margin-based criterion and is very robust to the Hughes phenomenon but also it has been widely used by many researchers in this field. Owing to the local structures extracted, Folded-PCA has the potential to improve the efficacy in feature selection thus expect to give better classification results. Next step can be dimension reduction using rough set, which has been suggested for reducing the dimensionality of nominal datasets.

REFERENCES

[1] Jaime Zabalza, Jinchang Ren, Mingqiang Yang, Yi Zhang, Jun Wang, Stephen Marshall, Junwei Han, "Novel Folded-PCA for Improved Feature Extraction and Data Reduction with Hyperspectral Imaging and SAR in Remote Sensing," ISPRS Journal of Photogrammetry and Remote Sensing 93 (2014) 112–122.

[2] Zhang Hao, Song Heng-jia, Yu Bo-chun, "Application of Hyper Spectral Remote Sensing for Urban Forestry Monitoring in Natural Disaster Zones," 2011 IEEE.

[3] Lori Mann Bruce, Cliff H. Koger, and Jiang Li, "Dimensionality Reduction of Hyperspectral Data Using Discrete Wavelet Transform Feature Extraction," IEEE Transactions on Geoscience and Remote Sensing, Vol. 40, NO. 10, October 2002.

[4] Antonio Plaza, Pablo Martínez, Javier Plaza, and Rosa Pérez, "Dimensionality Reduction and Classification of Hyperspectral Image Data Using Sequences of Extended Morphological Transformations," IEEE Transactions on Geoscience and Remote Sensing, vol. 43, no. 3, March 2005.

[5] Anish Mohan, Guillermo Sapiro, and Edward Bosch, "Spatially Coherent Nonlinear Dimensionality Reduction and Segmentation of Hyperspectral Images," IEEE Geoscience and Remote Sensing Letters, vol. 4, no. 2, April 2007.

[6] Jing Wang, and Chein-I Chang, "Independent Component Analysis-Based Dimensionality Reduction with Applications in Hyperspectral Image Analysis," IEEE Transactions on Geoscience and Remote Sensing, vol. 44, no. 6, June 2006.

[7] Charles M. Bachmann, Thomas L. Ainsworth, and Robert A. Fusina, "Exploiting Manifold Geometry in Hyperspectral Imagery," IEEE Transactions on Geoscience and Remote Sensing, vol. 43, no. 3, March 2005.

[8] Rouhollah Dianat and Shohreh Kasaei, "Dimension Reduction of Optical Remote Sensing Images via Minimum Change Rate Deviation Method," IEEE Transactions on Geoscience and Remote Sensing, vol. 48, no. 1, January 2010.

[9] Kitti Koonsanit, Chuleerat Jaruskulchai, and Apisit Eiumnoh, "Band Selection for Dimension Reduction in HyperSpectral Image Using Integrated Information Gain and Principal Components Analysis Technique," International Journal of Machine Learning and Computing, vol. 2, no. 3, June 2012.

[10] Ufuk Sakarya, "Hyperspectral Dimension Reduction Using Global and Local Information Based Linear Discriminant Analysis," ISPRS Annals of the Photogrammetry, Remote Sensing and Spatial Information Sciences, volume II-7, 2014.

[11] Wei Li, Saurabh Prasad, James E. Fowler, and and Lori Mann Bruce, "Locality-Preserving Dimensionality Reduction and Classification for Hyperspectral Image Analysis," IEEE Transactions on Geoscience and Remote Sensing, vol. 50, no. 4, April 2012.

[12] SU Junying, and Shu Ning, "A Dimensionality Reduction Algorithm of Hyper Spectral Image Based on Fract Analysis," The International Archives of the Photogrammetry, Remote Sensing and Spatial Information Sciences. vol. XXXVII. Part B7. Beijing 2008.

[13] Qazi Sami ul Haq,Lixin Shi,Linmi Tao,Shiqiang Yang, "A Robust Band Compression Technique for Hyperspectral Image Classification," IEEE 2010.

[14] Jinn-Min Yang, Pao-Ta Yu, Bor-Chen Kuo, and Ming-Hsiang Su, "Nonparametric Fuzzy Feature Extraction for Hyperspectral Image Classification," International Journal of Fuzzy Systems, vol. 12, no. 3, September 2010.

[15] Joseph C. Harsanyi, and Chein-I Chang, "Hyperspectral Image Classification and Dimensionality Reduction: An Orthogonal Subspace Projection Approach," IEEE Transactions on Geoscience and Remote Sensing, vol. 32, no. 4, July 1994.

[16] Craig Rodarmel and Jie Shan, "Principal Component Analysis for Hyperspectral Image Classification," Surveying and Land Information Systems, vol. 62, no. 2, 2002.

[17] J.S. Borges & A.R.S. Marc¸al, J.M.B. Dias, "Evaluation of feature extraction and reduction methods for hyperspectral images," New Developments and Challenges in Remote Sensing, Z. Bochenek (ed.), 2007.

[18] Bijith Marakarkandy,Dr. B.K. Mishra, "Issues in Dimensionality Reduction of Multispectral and Hyperspectral data," International Journal of Computer Science and Information Technologies, vol. 2 (5) , 2011, 1847-1851.

[19] Qian Du and J.E.Fowler, "Hyperspectral Image Compression using JPEG-2000 and Principal Component Analysis," IEEE Geosci. Remote Sens. Lett. vol.4 no 2, April, 2007.

[20] Xiuping Jia, and John A. Richards, "Segmented Principal Components Transformation for Efficient Hyperspectral Remote-Sensing Image Display and Classification," IEEE Transactions on Geoscience and Remote Sensing, vol. 37, no. 1, January 1999.

[21] Qian Du, Wei Zhu, He Yang, and James E. Fowler, "Segmented Principal Component Analysis for Parallel Compression of Hyperspectral Imagery," IEEE Geoscience and Remote Sensing Letters, vol. 6, no. 4, October 2009.

[22] Nutan C.Malekar, Dr.R.R.Sedamkar, "Novel K-Means Clustering Approach for Compressing Hyperspectral Image," International Journal of Advancements in Research & Technology, volume 3, Issue 1, January-2014.

[23] Nicola Falco, Jón Atli Benediktsson, and Lorenzo Bruzzone, "A Study on the Effectiveness of Different Independent Component Analysis Algorithms for Hyperspectral Image Classification," IEEE Journal of Selected Topics in Applied Earth Observations and Remote Sensing, vol. 7, no. 6, June 2014.

[24] S. Esakkirajan, T. Veerakumar, Adabala N. Subramanyam, and C. H. PremChand, "Removal of High Density Salt and Pepper Noise Through Modified Decision Based Unsymmetric Trimmed Median Filter," IEEE Signal Processing Letters, vol. 18, no. 5, May 2011.

[25] Chein-I Chang, and Qian Du, "Interference and Noise-Adjusted Principal Components Analysis," IEEE Transactions on Geoscience and Remote Sensing, vol. 37, no. 5, September 1999.

[26] http://aviris.jpl.nasa.gov/data/free_data.html

[27] http://compression.jpl.nasa.gov/hyperspectral/

LIST OF PUBLICATIONS

Conferences

- Presented a paper titled "Data Reduction Techniques of Hyperspectral Images: A Comparative Study" in the 3rd International Conference on Signal Processing, Communications and Networking (ICSCN) held during 26^{th} – 28^{th} , March 2015, organized by Madras Institute of Technology, Chennai.
- Presented a paper titled "Feature Extraction of Hyperspectral Image Using Principal Component Analysis and Folded-Principal Component Analysis" in 2nd International Conference on Electronics and Communication Systems (ICECS 2015) on 26^{th} and 27^{th} February,2015 organized by Karpagam College of Engineering, Coimbatore.